Published in final edited form as:

Neurobiol Aging. 2021 January ; 97: 73–88. doi:10.1016/j.neurobiolaging.2020.10.001.

Alzheimer amyloid-β- peptide disrupts membrane localization of glucose transporter 1 in astrocytes: implications for glucose levels in brain and blood

Rachel D. Hendrix[a,1], **Yang Ou**[b], **Jakeira E. Davis**[c], **Angela K. Odle**[a], **Thomas R. Groves**[a,2], **Antiño R. Allen**[a,d], **Gwen V. Childs**[a], **Steven W. Barger**[a,b,e,*]

[a]Department of Neurobiology & Developmental Sciences, Little Rock, AR, USA

[b]Department of Geriatrics, Little Rock, AR, USA

[c]Graduate Program in Interdisciplinary Biomedical Sciences, Little Rock, AR, USA

[d]Department of Pharmaceutical Sciences, University of Arkansas for Medical Sciences, Little Rock, AR, USA

[e]Geriatric Research, Education & Clinical Center, Central Arkansas Veterans Healthcare System, Little Rock, AR, USA

Abstract

Alzheimer's disease (AD) is associated with disturbances in blood glucose regulation, and type-2 diabetes elevates the risk for dementia. A role for amyloid-β peptide (Aβ) in linking these age-related conditions has been proposed, tested primarily in transgenic mouse lines that overexpress mutated amyloid precursor protein (APP). Because APP has its own impacts on glucose regulation, we examined the BRI-Aβ42 line ("$A\beta_{42}$-tg"), which produces extracellular $A\beta_{1–42}$ in the CNS without elevation of APP. We also looked for interactions with diet-induced obesity (DIO) resulting from a high-fat, high-sucrose ("western") diet. $A\beta_{42}$-tg mice were impaired in both spatial memory and glucose tolerance. Although DIO induced insulin resistance, $A\beta_{1–42}$ accumulation did not, and the impacts of DIO and Aβ on glucose tolerance were merely additive. $A\beta_{42}$-tg mice exhibited no significant differences from wild-type in insulin production, body

*Corresponding author at: Department of Geriatrics, University of Arkansas for Medical Sciences, 629 Jack Stephens Dr, Ste. 4150, Little Rock, AR 72205, USA. Tel.: +1 501 526 5811; fax: +1 501 526 5830. bargerstevenw@uams.edu (S.W. Barger).

[1]Present address: Department of Neurology, Washington University, St. Louis MO.

[2]Present address: Axiom (Huntsworth Health), Yardley PA.

Credit author statement: Steve Barger conceived of the study, performed some of the experiments, advised others, and contributed substantively to the text. Rachel Hendrix performed many of the experiments and was primary author of the text. Yang Ou performed most of the analysis of glucose transporters, including cell fractionation. Jakeira Davis performed experiments with primary astrocyte cultures. Angela Odle trained Dr Hendrix in the use of CLAMS cages. Thomas Groves performed the Morris water maze assessments and contributed to analysis of those data. Antiño Allen trained Dr Groves, designed aspects of the behavioral assessments, and contributed to analysis of those data. Gwen Childs provided the CLAMS cages and advice on that aspect of the study. All authors reviewed the text and made contributions to its final form.

Disclosure statement

S.W.B. has received royalties from Millipore-Sigma related to sales of secreted amyloid precursor proteins. No products related to such royalties were used in this study.

Appendix A. Supplementary data

Supplementary data to this article can be found online at https://doi.org/10.1016/j.neurobiolaging.2020.10.001.

weight, lipidemia, appetite, physical activity, respiratory quotient, an-/orexigenic factors, or inflammatory factors. These negative findings suggested that the phenotype in these mice arose from perturbation of glucose excursion in an insulin-independent tissue. To wit, cerebral cortex of $A\beta_{42}$-tg mice had reduced glucose utilization, similar to human patients with AD. This was associated with insufficient trafficking of glucose transporter 1 to the plasma membrane in parenchymal brain cells, a finding also documented in human AD tissue. Together, the lower cerebral metabolic rate of glucose and diminished function of parenchymal glucose transporter 1 indicate that aberrant regulation of blood glucose in AD likely reflects a central phenomenon, resulting from the effects of Aβ on cerebral parenchyma, rather than a generalized disruption of hypothalamic or peripheral endocrinology. The involvement of a specific glucose transporter in this deficit provides a new target for the design of AD therapies.

Keywords

Alzheimer's disease; Amyloid β-peptide; Astrocytes; Diabetes mellitus; Type 2; Glucose; Glucose transporter type 1; Obesity

1. Introduction

Alzheimer's disease (AD) is classically characterized by the histopathologic presence of amyloid-β plaques and tau tangles within the AD brain, but there is a growing appreciation for associated somatic pathologies (Folch et al., 2018). For instance, the prevalence of either impaired glucose tolerance or type-2 diabetes (T2D) is higher in patients with AD (Janson et al., 2004; Ohara et al., 2011), although this finding is not consistent across cohorts (Thambisetty et al., 2013). Despite this tendency toward elevated blood glucose concentration ($[Glc]_b$), patients with AD exhibit a decrease in cerebral metabolic rate of glucose (CMR_{glc}) (Gabel et al., 2010; Hoffman et al., 2000). Although T2D is also associated with diminished CMR_{glc} (Baker et al., 2011), this disorder does not appear to exacerbate accumulation of amyloid-β peptide (Aβ) (Peila et al., 2002; Roberts et al., 2014), suggesting that T2D does not predispose to AD.

The mechanism by which diabetic conditions cause a decline in CMR_{glc} has been investigated in animal models and a limited number of human studies. A considerable number of studies have documented diminished expression and/or activity of glucose transporters in brain endothelium in response to chronic hyperglycemia and/or diet-induced obesity (DIO) (Cornford et al., 1995; Gjedde, 1981; Jais et al., 2016; Lutz and Pardridge, 1993; Mooradian and Morin, 1991; Pardridge et al., 1990). In most cases, this phenomenon has been traced to a reduction in endothelial expression of glucose transporter 1 (GLUT1), the primary glucose transporter in cerebrovasculature. Whereas other tissues are bathed in high glucose under diabetic conditions, the brain—owing to the restrictions of the blood-brain barrier (BBB)—suffers a reduction in CMR_{glc} when there is a reflexive downregulation of glucose transporters in the cerebrovasculature (Baker et al., 2011; Boyle et al., 1995; Roberts et al., 2014). Attempts to characterize transporter levels or function in AD and its models have been less consistent and detailed.

To explore relationships between AD and somatic glucose regulation, we probed the physiological status of a mouse model that accumulates Aβ in the CNS. Previous studies of these parameters have relied primarily on models of AD that overexpress mutant forms amyloid precursor protein (APP) and other APP peptide fragments formed from proteolytic cleavage. Our studies (Kulas et al., 2019) and those of others (Botteri et al., 2018; Needham et al., 2008; Tu et al., 2012) indicate that APP has direct effects on insulin and glucose regulation independent of Aβ. Because the vast majority of AD cases are sporadic and derive from accumulations of Aβ without APP mutation or overexpression, we investigated glucose regulation in a model that accumulates $A\beta_{1–42}$ alone: the BRI-Aβ42 mouse line (McGowan et al., 2005). For comparison with circumstances in which metabolic syndrome prevails, we invoked DIO through feeding “western” diet. We find that overproduction of human $A\beta_{1–42}$ in mice is sufficient to produce reductions of peripheral glucose tolerance and CMR_{glc}. This glucose perturbation was independent of insulin resistance, insulin deficiency, obesity, an-/orexigenic hormones, and overt inflammatory events. Through a diverse, multifaceted set of experiments, we conclude that the elevation of blood glucose levels resulting from Aβ production is explained primarily by reduced transport of glucose into the brain due to aberrant subcellular localization of GLUT1 in brain parenchyma with no apparent involvement of vascular transporters.

2. Materials and methods

2.1. Human tissue

Specimens were obtained from a brain bank maintained locally which catalogs and characterizes autopsy material from the University of Arkansas for Medical Sciences UAMS Department of Pathology and the Central Arkansas Veterans Healthcare System Pathology Service. They were acquired from autopsies of individuals diagnosed as AD (without Parkinson’s disease or mixed Lewy body pathology) or age-matched controls (AMC), as per National Institute on Aging-Reagan guidelines (Montine et al., 2012), which incorporate consortium to establish a registry for Alzheimer’s disease evaluation of neuritic plaque density and Braak & Braak staging of neurofibrillary tangles. Samples were obtained by 3-D dissection of autopsy-provided material from left prefrontal cortex, which were flash frozen in N_2 (l) and stored at −80 °C. Specimens did not qualify as human subject research as per US Department of Health and Human Services Exemption 4. The N = 10 for each group. Average age of the AD cases was 81.1 year old, and they were 40%/60% female/male; the AMC cases were 83.0 year old and 30%/70% female/male; each group was 9:1 Caucasian:African-American. Postmortem intervals were 5 and 9 hours for AD and AMC, respectively.

2.2. Animals

Each protocol was approved by the Institutional Animal Care and Use Committee of the Central Arkansas Veterans Healthcare System (CAVHS) or of the UAMS. Mice were housed in a 12-h light/dark cycle at 23°C at the AAALAC-certified CAVHS vivarium unless otherwise noted. A normal diet (ND) and water was provided *ad libitum* (kcal: 22% protein, 16% fat, and 62% carbohydrates; LabDiet JL Rat and Mouse/6FOvals w/Hysil; 5k67-RHI-W 30). Mice were weaned at age 25 days or older and housed at a cage density of ≥82 cm/

mouse of floor space. Both sexes were evaluated in some assessments, but females showed no effect of genotype or diet, so only data from male mice are presented here.

Hemizygous BRI-Aβ42 ($A\beta_{42}$-tg) transgenic mice [(McGowan et al., 2005); akin to MMRRC stock: #34842] were provided by Dr Todd Golde (University of Florida). The transgene is a fusion construct in which the $A\beta_{1–42}$ sequence replaces the C-terminal 23 amino acids of the BRI British dementia protein, directing a proteolytic liberation of $A\beta_{1–42}$ into the extracellular space, without overexpression of APP. The prion promoter construct used in this line results in transgene expression primarily in the CNS (Borchelt et al., 1996), and plasma levels of Aβ in the BRI-Aβ42 line are ~100-fold below those in an APP-transgenic line (Levites et al., 2006). All analyses were performed on mice hemizygous for the transgene. With the exception of the adrenalectomy study, all mice were backcrossed to C57BL/6N wild-type (WT, Harlan) to produce WT and $A\beta_{42}$-tg littermates that were $Nnt^{+/+}$ (as C57BL/6J are $Nnt^{-/-}$). Adrenalectomized mice were obtained from the Jackson Laboratory (Bar Harbor, ME) in a stock that had been maintained in C57BL/6J (JAX stock: #007182). Genotyping was performed by PCR for the transgene with the following primers: 5′- AAG GCT GGA ACC TAT TTG CC −3′ and ‘5- TAG TGG ATC CCT ACG CTA TG −3’ (307-bp product). A T-cell receptor gene was used in a positive-control reaction with the following primers: 5′- CAA ATG TTG CTT GTC TGG TG-3′ and 5′- GTC AGT CGA GTG CAC AGT TT −3’ (200 bp).

2.3. Diet-induced obesity

To test for interactions between the glycemic effects of Aβ and those of DIO, we feed some mice western diet (WD; EnvigoTeklad TD.88137; kcal: 15% protein, 42% fat, 43% carbohydrate), an obesogenic nutritional source high in sucrose (34% by weight) and milk fat. Mice were split into four experimental groups: WT ND, WT WD, $A\beta_{42}$-tg ND, and $A\beta_{42}$-tg WD. At week 0, all mice were 6 week old ±3 days. Glucose tolerance tests (GTTs) and insulin tolerance tests (ITTs), both detailed below, were administered on alternating weeks to reduce handling stress effects. After the first ITT on week 1, half of each litter had the normal chow diet replaced with the WD. They were maintained on the diet until euthanasia at diet week 20. In addition to GTTs and ITTs, these mice were used for data on insulin production, hypothalamic gene expression, and circulating and tissue levels of hormones and cytokines.

2.4. Glucose, insulin, and pyruvate tolerance testing

Glucose tolerance was assessed through an intraperitoneal administration of glucose followed by intermittent monitoring of blood glucose concentration ($[Glc]_b$) for 120 minutes. Before glucose tolerance testing, mice were fasted (with drinking water provided) for 5 h. The fasting was conducted primarily during the mornings, typically starting between 8 am and 9 am, with GTTs beginning between 1 pm and 2 pm. Mice were weighed, and 2 g/kg of D-(+)-glucose (Sigma, St. Louis, MO) in sterile water (Baxter Healthcare Inc, Deerfield, IL) was administered (190–230 μL total volume) intraperitoneally. The glucose solution was filtered using a 0.24-μm syringe filter before use. An AlphaTRAK 2 glucometer (Zoetis Inc, Kalamazzo, MI) was used to sample blood from the tip of the tail just before injection and at 15, 30, 60, and 120 minutes after injection. Total area under the

curve (tAUC) was calculated from a baseline of 0 mg/dL using the trapezoid rule. Incremental area under the curve (iAUC) was calculated by rendering the y-axis as the difference of each time point from the initial glucose reading for a given animal. Pyruvate tolerance testing was performed in a similar manner using 1 g/kg of 10% sodium pyruvate diluted in phosphate-buffered saline (PBS).

Insulin tolerance testing was performed in a similar manner as GTTs; however, mice were not fasted unless otherwise indicated. Insulin (Humulin R; Lily USA, Indianapolis, IN) was diluted in saline (Molecular Biologicals International, Irvine, CA) and administered ip at 0.35 U/kg. Because insulin evokes a downward deflection in $[Glc]_b$, the integral reported is area over the curve (AOC), calculated by rendering the y-axis as the absolute value of the difference of each time point from the initial glucose reading for a given animal.

2.5. Comprehensive lab animal monitoring system (CLAMS)

CLAMS cages (Oxymax; Columbus Instruments, Columbus OH) were used to assess several aspects of activity and metabolism, including food consumption and indirect calorimetry. A unique cohort of 13- to 17-week-old $A\beta_{42}$-tg mice and their WT littermates, distinct from those used in other assays, was evaluated in this paradigm. Mice were housed individually inside CLAMS cages at the UAMS facility with water and food *ad libitum* under a 14/10 hours light/dark cycle. The mice were acclimated for 21 hours before starting data collection, and data were collected for 48 hours. Body weights were obtained before and after the CLAMS session. The instrument simultaneously measures CO_2, O_2, food consumption, and 3-D physical movement. Energy expenditure and respiratory exchange ratio were calculated from the gas measurements. Activity was measured as the number of infrared beam breaks. The beams were stationed in the Z dimension to create two X-planes, one above the other, allowing inclusion of movement in the Z direction. Grooming and ambulation were recorded in aggregate based on the number beam breaks in the lower plane. Ambulation was differentiated by consecutive beam breaks in the lower plane and also recorded. Beam breaks in the upper plane (Z-axis) accounted for rearing and jumping movements. Sleep was defined by relatively prolonged periods of inactivity and has been validated with an 88%–94% agreement with electroencephalogram and video analysis (Pack et al., 2007).

2.6. Morris water maze (MWM)

A unique cohort of mice housed at the UAMS facility was assessed for spatial memory via MWM as described previously (Alexander et al., 2018). At 10 weeks of age, 14 mice per genotype were randomized into two groups: ND or WD (above); groups of Aβ-tg mice and WT mice were all from the same litters. At 16 weeks of age, the mice were trained to locate a clearly marked platform (visible-platform training, days 1 and 2), confirming that groups were similar regarding swimming and learning ability. Start locations were changed for each trial. Swimming paths are recorded with an EthoVision XT video tracking system (Noldus Information Technology). Mice were subsequently trained to locate the platform hidden beneath the surface of the opaque water (hidden-platform training, days 3–5). Mice were trained 4–8 times a day for 5 days. After training, a probe trial was conducted on day 6 comprising 60 seconds without a platform; the outcome measure was time spent in each

quadrant of the pool. During the course of this testing, animals were maintained on their respective diets.

2.7. Assessment of adrenalectomized mice

To evaluate contributions of the hypothalamic-pituitary-adrenal (HPA) axis to the glycemic effects of Aβ, adrenalectomy was performed on BRI-Aβ42 mice [B6.Cg-tg(Prnp-ITM2B/APP695*42) A12Emcg/J; stock no. 007182] and WT littermates at 5.5 weeks of age by the Jackson Laboratory (Bar Harbor, ME); unoperated littermates were provided at the same time (6 per group). They were maintained on an *ad libitum* ND, and adrenalectomized mice were provided a 0.9% saline solution to counter the effects of mineralocorticoid deficiency on kidney function (Bristol and Drill, 1952). The animals were shipped to the CAVHS facility and allowed to acclimate for one week before testing. In one-week intervals, they underwent GTTs, ITTs, and a GTT in which blood was collected via retro-orbital eye bleed to measure insulin response to glucose challenge at 0 and 30 minutes. The following week all animals were euthanized. One $A\beta_{42}$-tg adrenalectomized and two WT adrenalectomized mice died during the second GTT. The DetectX Corticosterone Enzyme Immunoassay Kit (Arbor Assays) was used to compare circulating levels of glucocorticoids in serum of adrenalectomized mice at the time of euthanasia.

2.8. Tissue collection

Mice were rapidly anesthetized using intraperitoneal injection of 250 mg/kg sodium pentobarbital (Nembutal, Oak Pharmaceuticals or Diamondback Drugs). Blood was taken from the left and right ventricles of the heart in a heparinized syringe and placed on ice. A 50 μL aliquot was mixed with protease inhibitors. Blood was then centrifuged at 7500*g* for 15 minutes at 4 °C, and the resulting serum layer was carefully pipetted and stored at −80 °C. Mice were perfused with heparinized (50 U/mL) saline for approximately 5 minutes, when clear saline solution was leaving the body cavity and the liver appeared to blanch. The brain was extracted, and the hypothalamus, right cortex, and right hippocampus were flash frozen in liquid nitrogen. The left half brain was fixed by immersion in 10% formalin.

2.9. Comprehensive metabolic panel

The Piccolo Comprehensive Metabolic Panel and Piccolo Xpress chemistry analyzer were used to assess the concentration of alanine aminotransferase, albumin, alkaline phosphatase, amylase, calcium, creatinine, glucose, phosphorous, potassium, sodium, total bilirubin, total globulin, total protein, and blood urea nitrogen in heparinized whole blood. Blood was collected during euthanasia into a sodium heparinized tube, and 100 μL was added to each panel disc.

2.10. ELISA for insulin and Aβ

Serum was collected from the tail vein of the cohort of mice used for DIO analysis, including the corresponding ND animals (above). Insulin levels were also assessed in eye bleeds from the cohort used for adrenalectomy, including the unoperated animals (above). Mice were fasted and injected with glucose as per the GTT assays. Blood was collected before and 30 minutes after injection, and it was allowed to clot before collection of serum

by centrifugation. Insulin was measured using an Insulin Mouse Ultrasensitive ELISA (Crystal Chem Inc) as per manufacturer's instructions for the wide range assay (0.1–12.8 ng/mL). Standards and samples were assayed in duplicate. Data points for individual samples in which a coefficient of variability between duplicates was greater than 20% were excluded. $A\beta_{1-42}$ was extracted from brain, plasma, and other tissues in three steps to yield fractions soluble in buffered saline, Triton X-100, and formic acid (McDonald et al., 2012). The peptide was measured in each fraction by Quantikine ELISA Kit (R&D Systems), as per manufacturer's instructions.

2.11. Cerebral metabolic rate of glucose (CMR_{glc}) measurements

To test whether $A\beta_{42}$-tg mice showed deficits in CMR_{glc} as seen in other AD mouse models and AD itself, we assayed the accumulation of [^{3}H]2-deoxyglucose (2-DG) and its primary metabolite in the cerebral cortex of $A\beta_{42}$-tg mice and WT littermates. Unanesthetized 15-week-old mice were acclimated to a restraint tube by 45-second restraint sessions conducted daily for one week. On the day of assay, 100 μCi/kg [^{3}H]2-DG and 10 μCi/kg [^{14}C]sucrose was injected into the lateral tail vein. Blood was collected from a separate (distal) tail site at 3, 7, 11, and 15 minutes after injection into heparinized tubes. Mice were euthanized via decapitation immediately after the final time point, trunk blood was collected in a tube containing heparin, and brain was quickly dissected and snap-frozen. Both hemispheres of the cerebral cortex were homogenized in radio-immunoprecipitation (RIPA) buffer (150 mM NaCl, 50 mM Tris HCl, 1 mM EDTA, 1% Triton X-100, 0.5% sodium deoxylcholate, 0.1% SDS, pH 7.4) and extracted with 65% ethanol. Liquid scintillation counting was used to measure cpm of ^{3}H and ^{14}C in plasma and in the soluble and insoluble fractions of tissue. CMR_{glc} was calculated based on the study by Vallerand et al. (1987). Specifically, the extracellular volume (in μL/mg) was calculated by dividing the amount of brain ^{14}C (dpm per milligram of tissue) by the amount of ^{14}C in blood (dpm per μL of plasma) at the time of death. The amount of extracellular [^{3}H]2-DG (dpm per mg of tissue) was obtained by multiplying the extracellular volume (in μl per mg of tissue) by the blood concentration of [^{3}H]2-DG (dpm per μl of plasma) at the time of death. This blood concentration of [^{3}H]2-DG (dpm per mg of tissue) was subtracted from the total concentration to obtain the parenchymal concentration of [^{3}H]2-DG (dpm per mg of tissue).

2.12. Quantitative real-time PCR

Tissue was homogenized in Qiagen RLT buffer using a Lysing Matrix D tube (MP Biomedicals; component of FastRNA Green Kit) and the FastPrep-24 instrument (MP Biomedicals) on setting "6" for 2 × 20 seconds. Lysate was centrifuged at 16,300*g* for 1 minute. Samples were transferred to a new tube and spun again for 3 minutes before carefully adding supernatant to a gDNA Eliminator spin column of the RNeasy Plus Mini Kit (Qiagen), and the RNA was extracted following the kit instructions. The quality of the RNA was assessed using the Agilent 2100 Bioanalyzer. All samples had an RNA integrity number greater than 7. A two-step RT-PCR protocol was used; RT (cDNA synthesis) was completed using the ImProm-II Reverse Transcription System (Promega) and random hexamer primers. A portion of each sample was pooled and serially diluted to form a standard curve for absolute quantification. Samples were diluted to fall within the center of the standard curve and combined with primers (Supplemental Table 1) and SYBR Green

PCR Master Mix (Applied Biosystems) for amplification and detection using an ABI 7900HT Fast Real-Time PCR System. *Rplp0*, reported to be a stably expressing transcript in the hypothalamus under various diabetic conditions (Li et al., 2014), was used as a reference gene in all experiments. All reactions used the following three-stage protocol: Incubation/denaturation: 50 °C for 2:00/95 °C for 10:00; PCR amplification for 50 cycles: 95 °C for 0:15, 55 °C for 0:15, and 72 °C for 1:00; and melt curve: 95 °C for 0:15, 60 °C for 1:00, and 95 °C for 0:15.

2.13. GLUT1 determinations by SimpleWes

Glucose transport and utilization can be dramatically affected by changes in the subcellular distribution from intracellular stores to the plasma membrane. To determine if this contributed to differences in glucose uptake in AD or in $A\beta_{42}$-tg mice, we optimized conditions for separation of plasma membrane fractions and for resolution/detection of various GLUT isoforms. Tissue from cerebral cortex of human subjects and most mouse brains was pulverized in with mortar and pestle chilled in liquid nitrogen, and the powder was mixed to homogeneity.

For a subset of mice, brain microvessel isolates were prepared, making use of both cerebral hemispheres. After dissection from the skull and other brain regions, the hemispheres were carefully stripped of meningeal tissue while in ice-cold PBS, then Dounce-homogenized on ice in 0.6 mL Buffer D [2.7 mM KCl, 1.46 mM KH_2PO_4, 136.9 mM NaCl, 8.1 mM Na_2HPO_4, 5 mM D-glucose, 1 mM sodium pyruvate, 0.9 mM $CaCl_2$, 0.5 mM $MgCl_2$, and 5 mg/mL protease inhibitors (Pierce Mini Tablets, EDTA-free), pH 7.4]. The homogenate was mixed 1:1 with 30% Ficoll and centrifuged at 5800 × *g* for 15 minutes at 4 °C. The supernatant was discarded, and the pellet was resuspended in 1 mL of another 1:1 mixture of Buffer D and 30% Ficoll. After another centrifugation at 5800 × *g* for 15 minutes at 4 °C, the supernatant was discarded and the pellet was resuspended in Buffer D and centrifuged at 1000 × *g* for 3 minutes at 4 °C. The supernatant was discarded, and the pellet was stored at −80 °C.

Pulverized tissue, microvessel isolates, and cultured astrocyte pellets were processed via the Minute Plasma Membrane Protein Isolation and Cell Fractionation Kit as per the instructions from the manufacturer (Invent Biotechnologies, Plymouth MN) to separate plasma membrane from the remainder (cytosol plus organelle membranes). We confirmed identity of the fractions by exclusive detection of plasma membrane calcium ATPase, sarcoplasmic/endoplasmic calcium ATPase, and β-actin in their expected fractions.

Fractions were analyzed for GLUT1 protein using the SimpleWes capillary electrophoresis instrumentation (Protein Simple, San Jose CA). Fractions from mouse cortical preparations were loaded at 1.4 mg/mL; anti-GLUT1 antibody (rabbit monoclonal EPR3915; abcam, Cambridge MA) was loaded at a 1:50 dilution. Fractions from mouse microvessel isolates were loaded at 0.2 mg/mL, and remainder fractions were loaded at 0.47 mg/mL. For human samples, plasma membrane fractions were loaded at 1.8 mg/mL, and remainder fractions were loaded at 0.32 mg/mL; antibodies were loaded recognizing GLUT1 (1:50), −3 (1:100), or −4 (1:20). For samples from astrocyte cultures, plasma membrane fractions were loaded at 0.22 mg/mL, and remainder fractions were loaded at 0.41 mg/mL; anti-GLUT1 antibody

was loaded at a 1:50 dilution. Gaussian peak integration was performed on the chemiluminescence values along the length of the capillaries, with peaks at ~45 kDa and ~55 kDa analyzed separately for GLUT1.

2.14. Primary cultures of astrocytes

Mixed-glia cultures were established from neonatal Sprague-Dawley rats as described previously (McMullan et al., 2012). The cultures were maintained in the Minimal Essential Medium (Earle's salts) supplemented to 10% with fetal bovine serum for 10–14 days. Microglia were removed by physical dislodgement, including aggressive lavage. Astrocytes were then trypsinized, subcultured in 15-cm plates in the Minimal Essential Medium /fetal bovine serum. Characterization of these cultures with cell type-specific antibodies demonstrated them to be ≥95% astrocytes (Supplement Fig. 1). The cultures were treated after they had reached 90% confluency. Lysates were prepared with the Minute Plasma Membrane Protein Isolation and Cell Fractionation Kit as per the instructions from the manufacturer (Invent Biotechnologies, Plymouth MN) to produce plasma membrane and cytosolic fractions.

$A\beta_{1–42}$ (Anaspec) was dissolved at 1 mM 4 hours in hexafluoroisopropanol, aliquoted, and evaporated to dry; it was stored under desiccant at −80 °C. For aggregation, an aliquot was dissolved at 2 mM in anhydrous dimethylsulfoxide, and then diluted to 150 μM in PBS at 4 °C. The peptide was incubated in PBS at 4 °C for 24 hours before use.

2.15. Immunofluorescence

Primary astrocyte cultures were plated onto glass coverslips coated with rat tail collagen. After treatment, the cultures were fixed for 15 minutes in ice-cold PBS containing 4% paraformaldehyde, followed by three washes with PBS. Some cultures were permeabilized by application of PBS containing 0.3% Tween-20 at room temperature for 30 minutes, followed by three washes with PBS; other cultures were subjected immediately to blocking without permeabilization. Blocking comprised exposure for 1 hour to blocking solution: PBS containing 1% fatty acid-free bovine serum albumin. Primary antibody against GLUT1 (1:300; GT14-A, Alpha Diagnostic International, San Antonio TX), glial fibrillary acidic protein (1:1000; ab53554, Abcam), Iba1 (1:1000; 013-27,691, FUJIFILM Wako), pan-neuronal marker (1:25; MAB2300, Millipore-Sigma), phosphotyrosine (1:100; 05-947, Millipore-Sigma), S100B (1:200; NCL-S100p, Novocastra), or VE-cadherin (1:25; #36-1900, ThermoFisher) was applied for 2 hours at room temperature in blocking buffer, followed by three washes with PBS. Secondary antibodies were Alexa Fluor 488 donkey anti-rabbit (for GLUT1, S100, and VE-cadherin) and Alexa Fluor 594 donkey anti-goat (for GFAP) or anti-mouse (for Iba1, pan-neuronal, and phosphotyrosine), applied for 1 hour at room temperature in blocking buffer (1:500), followed by three washes with PBS. Coverslips were mounted onto microscope slides with ProLong Gold Antifade Mountant containing DAPI (ThermoFisher). Images were acquired with a Nikon Eclipse Ti using an Illuminator Sola and excitation/emission (nm) pairs of 360/460 (DAPI), 480/535 (AF488), and 560/630 (AF594). The camera was an Andor Zyla 5.5 sCMOS. For quantitative comparisons of GLUT1 across treatment conditions, consistent illumination intensity and acquisition times were used for all images.

2.16. Statistical analysis

For comparisons between two groups, Student's t-test with Welch's correction was used. One-way ANOVA with Bonferroni post hoc was used in assessing groups of 3 or more. Two-way ANOVA with Bonferroni post hoc was used in assessing multiple comparisons over time. Grubb's test was used to assess for outliers using GraphPad's online assessment tool (https://www.graphpad.com/quickcalcs/Grubbs1.cfm). All statistics were carried out using GraphPad Prism 7 software. Enzyme-linked immunosorbent assay (ELISA) curves were assessed using a four-parameter logistic regression curve (https://www.myassays.com/four-parameter-logistic-curve.assay).

3. Results

3.1. Spatial memory is impaired in $A\beta_{42}$-tg mice

Mouse models of Aβ accumulation in the CNS have shown impairments in spatial memory consistent with hippocampal deficits; several such models have also shown aberrations in regulation of peripheral glucose. However, many of these models rely on overexpression of APP, which appears to have effects on insulin and glucose dynamics itself. To exclude such contributions, we examined glucose regulation in the BRI-Aβ42 mouse ("$A\beta_{42}$-tg"), which releases $A\beta_{1–42}$ into CNS interstitial fluid without an APP transgene. This line also avoids any Aβ-independent effects of APP mutation; the latter may be more relevant for modeling familial AD than sporadic AD. $A\beta_{42}$-tg showed a deficit in spatial memory. Specifically, WT mice trained in the MWM showed a preference for the target quadrant during a probe trial (removal of escape platform after training), whereas their $A\beta_{42}$-tg littermates did not (Fig. 1).

3.2. Aβ overproduction influences systemic glucose homeostasis

Compared with WT littermates, $A\beta_{42}$-tg mice displayed impairments in an intraperitoneal GTT. Blood glucose levels ($[Glc]_b$) in $A\beta_{42}$-tg mice spiked to higher levels and were slower to recover, resulting in an increase in tAUC (Fig. 2A, B). After a 5-h fast, $A\beta_{42}$-tg mice also had a higher basal $[Glc]_b$ and trended toward a higher basal $[Glc]_b$ in the nonfasted (fed) state (Fig. 2C, D). The dynamic range of the response was calculated by subtracting the basal $[Glc]_b$ for each mouse individually to arrive at an iAUC. This value was also elevated significantly in $A\beta_{42}$-tg mice (Supplement Fig. 2). The following week, an ITT was performed to measure insulin sensitivity in the same cohort of mice. Because an ITT detects a decrease from baseline, integration of this parameter was performed as AOC. Responses in ITTs were equivalent in both genotypes (Fig. 2E, F). Likewise, no differences were detected in pyruvate tolerance tests, a measure of hepatic gluconeogenesis (Supplement Fig. 3).

3.3. DIO and Aβ have only additive effects on glucose intolerance

To test for potential interactions of Aβ with the diabetes-inducing aspects of obesity, WT and $A\beta_{42}$-tg mice were subjected to DIO through feeding a "WD." DIO was manifest as significant weight gain in all mice fed WD, regardless of genotype (Fig. 3A). DIO was also accompanied by hyperlipidemia and hypercholesteremia; total blood cholesterol levels were 61.5 ± 8.5 mg/dL in ND mice and 185.5 ± 32.9 mg/dL in DIO mice (mean ± SEM).

Impairments in GTTs and ITTs were observed in all DIO mice (Fig. 2A, B). Glucose intolerance developed over several weeks in DIO mice but was consistently present in $A\beta_{42}$-tg mice (Fig. 3B). Glucose tolerance was even further disrupted in DIO $A\beta_{42}$-tg mice, generally appearing as an additive effect of DIO and Aβ expression. Glucose levels in $A\beta_{42}$-tg mice were significantly different from WT at 60 minutes on either diet, but DIO had a stronger influence on glycemic rise overall. Basal $[Glc]_b$ was elevated in DIO $A\beta_{42}$-tg mice in both fasting and fed states (Fig. 2C, D), consistent with metabolic syndrome and incipient diabetes. DIO did not alter the levels of Aβ in any tissue assayed (mean: 8.9 ng/mg protein in cerebral cortex; 0.45 nM in plasma). DIO produced insulin resistance in both WT and $A\beta_{42}$-tg, reflected in the small AOC (Fig. 2E, F). By contrast, overexpression of $A\beta_{1–42}$ did not impair insulin tolerance (AOC) in either dietary condition (Fig. 2F).

We also tested the effects of DIO on memory performance. Consistent with prior reports (Jeon et al., 2012; Kasper et al., 2018; Lu et al., 2011; Mi et al., 2017), impaired performance was observed in DIO mice (Fig. 1). A combined effect of DIO and Aβ expression could not be detected because either alone removed essentially all preference for the target quadrant. Swim speed and distance swum were not impacted by diet or genotype. It is noteworthy that the mice began training at 16 weeks of age, at a time when soluble $A\beta_{1–42}$ is abundant in the CNS but approximately 7 months before the development of cerebral plaques.

3.4. Insulin production is not impaired in $A\beta_{42}$-tg mice

Blood was collected during the course of GTT on week 6 of the DIO study. Samples were taken immediately before (i.e., after a 5-h fast) and 30 minutes after an i.p. glucose administration, and insulin levels were measured in serum by ELISA. Mice fed an ND had similar fasting (T_0) insulin levels and responded to glucose with an elevation (Table 1); no significant differences were observed between genotypes. DIO mice of both genotypes showed hyperinsulinemia and poor responses to glucose. There was no significant difference between genotypes.

3.5. Hypothalamic control of glucose homeostasis appeared unaltered in $A\beta_{42}$-tg mice

The hypothalamus plays a key role in the coordination of circulating glucose, appetite, energy utilization, and fat metabolism. It is acted upon by both neurologic signals and humoral/endocrine factors; its output is similarly diverse. Based on the alterations in glucose handling revealed by the GTT, we chose to assess feeding behavior, activity cycles, sleep patterns, and energy metabolism using CLAMS cages.

Mice were acclimated in CLAMS cages for 20 h before 48 h of data collection during a 14/10-h light/dark period. Thirteen-week-old $A\beta_{42}$-tg mice consumed the same amount of food and were not different in body weight compared with their WT counterparts (Fig. 4A). Physical activity (motility) was equivalent between WT and $A\beta_{42}$-tg (Fig. 4B, a–b), and extrapolation of the beam breaks used for this assessment indicated no differences in time sleeping (Fig. 4B, C). The WT and transgenic mice did not differ by the amount of oxygen consumed or carbon dioxide expelled (Fig. 4C, a–d). Energy expenditure and respiratory

exchange ratio (reliance on carbohydrates for energy) did not differ by genotype (Fig. 4C, e–f).

A biochemical assessment of hypothalamic function may be achieved through measures of expression of relevant neuropeptides. The peptides themselves were below the level of reliable measurement without pooling tissue from multiple animals, so we analyzed mRNA in hypothalamic homogenates using qRT-PCR. The expression levels of *Agrp*, *Pomc*, and *Crh* and *Ptgs2* in 28-week-old mice were equivalent across genotype (Fig. 5A). Transcripts of receptors and signaling proteins *Insr*, *Irs1*, and *Mc4r*, all important to melanocortin system function, were also unaltered in $A\beta_{42}$-tg mice (Fig. 5B).

3.6. HPA axis contributions to Aβ-induced glucose intolerance

The HPA axis is one mechanism through which neurologic events can impact peripheral glucose levels. Because the hyperglycemic tendency of $A\beta_{42}$-tg did not appear to be insulin dependent, we tested whether a hyperactive HPA axis might be producing excessive glucocorticoids and thereby stimulating hepatic glucose production. $A\beta_{42}$-tg and WT mice were adrenalectomized ("$A\beta_{42}$-ADX" and "WT-ADX") and compared with unoperated littermates as controls ("$A\beta_{42}$-tg" and "WT"). Adrenalectomy decreased corticosterone levels in both genotypes (Fig. 6A). Because glucocorticoids can impact insulin production, we also measured circulating insulin levels in the adrenalectomized mice. Neither fasting insulin nor insulin level in response to glucose challenge differed between the groups (Supplement Fig. 4A). GTTs and ITTs were performed on these groups as described previously. Replicating our previous findings, $A\beta_{42}$-tg had had a slower decline in $[Glc]_b$ than WT, and this effect of Aβ expression was also apparent between genotypes within the ADX groups (Fig. 6B). Unoperated $A\beta_{42}$-tg mice had an impairment compared with unoperated WT in the tAUC, and iAUC showed a significant impairment in $A\beta_{42}$-tg mice compared with WT in both intact and ADX mice (Fig. 6C). ADX of both genotypes showed higher in $[Glc]_b$ than intact controls during ITTs, but Aβ expression again produced no effect on ITTs (Fig. 6D, Supplement Fig. 4B). After fasting, mice had no difference in basal $[Glc]_b$ (Fig. 6D).

3.7. Cerebral metabolic rate of glucose (CMR_{glc}) was diminished in $A\beta_{42}$-tg mice

The absence of any aberration in insulin production or sensitivity suggested that the impaired glucose tolerance in $A\beta_{42}$-tg mice may have resulted from aberrant utilization in an insulin-independent compartment, such as the CNS. AD is associated with reductions in CMR_{glc}, typically assessed in humans with fluorodeoxyglucose positron emission tomography (PET) imaging. To perform an equivalent assessment in mice, we performed $[^3H]$2-deoxyglucose uptake assays in 15-week-old WT and $A\beta_{42}$-tg mice. $[^{14}C]$Sucrose was coinjected to account for blood volume contributions. Blood samples from the tail vein were taken to measure the component of transport calculations dependent upon blood concentration. These measurements revealed that net $[^3H]$2-deoxyglucose uptake was lower in $A\beta_{42}$-tg mice than controls (WT K_i: 0.2259 ± 0.0354; $A\beta_{42}$-tg K_i: 0.1334 ± 0.0219; p = 0.043).

3.8. Aβ impairs translocation of GLUT1 to plasma membrane in astrocytes

Assessment of CMR_{glc} depends partially on the activity of hexokinase to trap the 2-DG intracellularly, but it occurs at concentrations of glucose below saturation of that enzyme. Therefore, CMR_{glc} appears to be dictated by rates of both phosphorylation and transport of glucose, the latter being a multiple step process dependent upon saturable transporters (Barros et al., 2005). Conceivably, differences in mobilization by other transporters within the brain parenchyma could also affect this process through shifting the glucose equilibrium. We assessed the state of GLUT1 and related transporters in cerebral cortex to determine whether impairment in one or more transporters might explain both the lower CMR_{glc} and the surfeit of $[Glc]_b$ in $A\beta_{42}$-tg mice. This venture was informed by proteomic analysis we recently performed on $A\beta_{42}$-tg and WT cerebral tissue that had been fractionated for membrane versus cytosolic fractions (Ayyadevara et al., 2019). Among those data, the membrane:cytoplasm ratio of GLUT1 was found to be reduced by 22% in $A\beta_{42}$-tg brain. Thus, in addition to total expression levels, we determined the fraction of transporter that was functionally localized by fractionating plasma membrane and comparing it with the remainder of cellular fractions. Steady-state levels of transporters in fractionated cerebral cortex of WT and $A\beta_{42}$-tg mice were assessed by a process of capillary electrophoresis coupled to immunodetection (“SimpleWes”) because of its sensitivity, quantitative validity, and commendable size resolution within the range of 40–60 kDa. Endothelial cells express a GLUT1 moiety migrating at 55 kDa, whereas CNS parenchymal cells express a 45-kDa GLUT1, considered to be primarily astrocytic. The proportion of 45-kDa GLUT1 at the plasma membrane was significantly lower in $A\beta_{42}$-tg than in WT cortical homogenates (Fig. 7A, C). No significant differences in 55-kDa GLUT1 were detected between WT and $A\beta_{42}$-tg mice (Fig. 7A, C). Attempts were made to perform similar analyses of other glucose transporters. GLUT2 could not be subjected to fractional calculation because plasma membrane levels in most specimens were below the level of detection, but total GLUT2 levels were reduced by 45% in the cortex of $A\beta_{42}$-tg mice (Fig. 7B). No difference was apparent in the fractional distribution of GLUT3 or GLUT4 (Fig. 7C). Total expression levels of all glucose transporters other than GLUT2 were similar across the genotypes (Supplement Fig. 5). GLUT1 and GLUT3 total levels were also unaltered in AD (Supplement Fig. 6).

The difference detected between 45-kDa and 55-kDa GLUT1 suggested that Aβ accumulation impacted GLUT1 trafficking in parenchymal cells but not in the vascular endothelial cells. To test this more directly, we performed microvessel isolation on the cortical tissue of WT and $A\beta_{42}$-tg mice; microvessels were then subjected to fractionation into plasma membrane and remainder. Similar to the results with total cortical homogenates, the membrane trafficking of the 55-kDa GLUT1 in this preparation was not different between WT and $A\beta_{42}$-tg (Fig. 7D).

Differences in total levels of GLUT1 have been reported in AD for some brain regions, but this does not appear to be a regionally consistent phenomenon (Vannucci et al., 1997). To determine if AD patients could suffer deficiencies in CMR_{glc} as a consequence of GLUT1 trafficking, we prepared membrane fractions of tissue homogenates from cerebral cortex of AD and AMC. As seen in the $A\beta_{42}$-tg mice, human AD cortical tissue showed a lower

distribution of 45-kDa GLUT1 to the plasma membrane (Fig. 7E). GLUT3 appeared to be unaffected, either in subcellular distribution or total levels.

To determine whether the lower plasma membrane fraction of GLUT1 could be a direct effect of Aβ, we treated primary cultures of astrocytes with oligomeric preparations of $A\beta_{1–42}$. Fractionated samples were assayed by SimpleWes as with cortical homogenates. After 6 hours of exposure to Aβ (5 μM), the 45-kDa GLUT1 present in these cultures showed a lower fractional partitioning to the plasma membrane than seen in control cultures (Fig. 8A). This effect was replicated by treatment with proinflammatory cytokines. Attenuated delivery of GLUT1 to the surface of Aβ-treated primary astrocytes was also detected by immunocytochemistry. Cultures were subjected to a mild fixation and immediately processed in either a permeabilized or unpermeabilized state, confirmed by differential detection of GFAP, an intracellular marker. Aβ treatment was associated with lower levels of GLUT1 on the surface or unpermeabilized cultures (Fig. 8B).

4. Discussion

An intriguing question arising from the dysregulation of glucose in AD is the extent to which this disorder's brain pathology and clinical symptoms arise secondary to peripheral events. A key aspect of human AD pathogenesis is a decrease in CMR_{glc}. Similar declines are seen in diabetics (both type-1 and type-2) and in animal models of chronic hyperglycemia. Other tissues experience a surfeit of glucose under such conditions, but the brain does not receive glucose passively; rather, it relies on saturable transporters at the BBB. A reactive downregulation of these transporters in response to hyperglycemia appears to contribute to the reduced CMR_{glc} seen in diabetic conditions. Accordingly, most evidence indicates that the cognitive impairment seen in T2D is attributable to vascular dementia rather than AD per se (Hassing et al., 2002; Matioli et al., 2017; Mortel et al., 1993; Pruzin et al., 2018; Raffaitin et al., 2009). This study explored the metabolic profile of mice that express human $A\beta_{1–42}$, a highly aggregative form of Aβ implicated in the pathogenesis of AD. We chose to avoid models relyingon overexpression and mutation of APP and presenilin, as each of these can have confounding effects on glucose metabolism (Botteri et al., 2018; Kulas et al., 2019; Lee et al., 2013; Needham et al., 2008; Tu et al., 2012). In contrast to those models, the $A\beta_{42}$-transgenic mice did not present with a generalized metabolic syndrome as might be expected if there were functional abnormalities in hypothalamic circuitry, peripheral hormones, adiposity, peripheral inflammation, or pancreatic insufficiency. They did, however, exhibit a cognitive deficit that was correlated with impaired glucose tolerance. Evaluation of cerebral glucose utilization suggested that the peripheral glucose phenotype of $A\beta_{42}$-tg mice—and perhaps their human counterparts—results from a CMR_{glc} impairment, itself due to an Aβ-induced irregularity in the translocation of GLUT1 to the plasma membrane in cells of the cerebral parenchyma. The perturbation of cerebral glucose was evident at ages much younger than that required for the observation of amyloid plaques in this line, indicating that it was driven by soluble Aβ.

Transgenic models of AD that overexpress APP have been reported to exhibit perturbations of general aspects of glucose and energy homeostasis, including impaired glucose tolerance, insulin resistance, and attenuated responses to leptin (Lyra E Silva et al., 2019). By contrast,

the peripheral phenotype of $A\beta_{42}$-tg was much more limited. While they had impaired glucose tolerance, $A\beta_{42}$-tg mice were not significantly heavier than WT. In T2D, impaired glucose tolerance is explained by a reduction in glucose uptake by peripheral tissues, initially as a consequence of insulin resistance in these tissues; this often progresses to a state of insufficient insulin production by pancreatic β-cells. $A\beta_{42}$-tg mice had a response to insulin equivalent to that of WT mice, indicating that their aberrant GTT results were not due to peripheral insulin resistance; insulin production was intact, as well. Moreover, our comprehensive metabolic panel demonstrated elevated glucose in the absence of biomarkers for hepatic or renal disorder. By these metabolic indices, $A\beta_{42}$-tg appear similar to humans with AD, who do not show differences from controls in body weight, insulin production, insulin sensitivity, or general hypothalamic function. Hepatic gluconeogenesis in response to pyruvate administration was similar in $A\beta_{42}$-tg and wild-type, suggesting that impaired GTTs did not arise from hepatic dysfunction. However, a small portion of the glucose intolerance was attenuated by adrenalectomy, indicating that elevated hepatic glucose production (perhaps by glycogenolysis) may have contributed weakly to the phenotype. AD, risk for AD, and cognitive impairment are all associated with elevations in cortisol levels (Ouanes and Popp, 2019).

We tested for hypothalamic contributions to the glucose phenotype of $A\beta_{42}$-tg mice through multiple approaches. Metabolic (CLAMS) cages were used to examine food consumption and respiratory quotient, the latter of which can detect differences in the degree to which energy production depends on carbohydrates versus other nutritional sources of energy. Infrared beam crossings in the cages permitted monitoring of physical activity, attributes of which were also extrapolated to inferences about sleep/wake behavior. These assessments indicated that the glucose tolerance of $A\beta_{42}$-tg mice was not associated with differences in diet, metabolism, activity, or sleep. This conclusion is supported by the failure to detect differences in transcriptional expression of melanocortin system neuropeptides that influence satiety and feeding.

Our 2-deoxyglucose measurements demonstrated that $A\beta_{42}$-tg mice phenocopy the decrease in CMR_{glc} seen in humans with AD. In the absence of other explanations, this diminished utilization by the most glucose-demanding organ is a plausible explanation for the exaggerated glucose excursions in $A\beta_{42}$-tg and the human disorder they model. While the human brain is only 2% of body mass, it may account for as much as 60% of our glucose utilization at rest (Berg et al., 2002). This percentage is smaller in mice, but rodent brains still create an outsized demand on glucose disposition (Sokoloff, 1977). Saturable glucose transporters limit access of this carbohydrate to the CNS, and diminutions in endothelial GLUT1 are well-documented in conditions of chronic hyperglycemia (Gjedde and Crone, 1981; McCall et al., 1982; Pardridge et al., 1990). AD and mouse models thereof do not universally exhibit hyperglycemia to a degree and consistency sufficient to downregulate endothelial GLUT1 expression. Indeed, we find this moiety unaltered. Instead, an isoform of GLUT1 specific to parenchymal cells appeared to be significantly lower in its functional localization. Astrocytic end-feet make canonical contributions to the neurovascular unit, and astroglia serve as a conduit for energy substrates from the vasculature to neurons, evidently supplying glucose and its derivatives to neurons (Dienel, 2012). Interruptions in this glucose flux are likely to 1) diminish neuronal function and 2) shift the equilibrium for central

import of glucose from blood. Together, the lower CMR_{glc} and mislocalization of parenchymal GLUT1 that we have detected suggest that elevations in blood glucose in AD reflect a central phenomenon, resulting from the effects of Aβ on cerebral parenchyma, rather than a generalized disruption of hypothalamic or peripheral endocrinology. Feasibility of this explanation is supported by the impaired glucose tolerance exhibited in mice lacking GLUT4 in neural tissues (Reno et al., 2017); however, that phenotype also included insulin resistance and other attributes suggesting that it involved impaired glucose sensing, likely in the hypothalamus.

It is clear that CMR_{glc} is correlated with cognitive performance. Decades of imaging studies have demonstrated that CMR_{glc} declines in patients with AD (Friedland et al., 1983; Herholz et al., 2007; Laforce et al., 2014; Leuzy et al., 2018). The phenomenon is also observed in essentially every syndrome of age-related dementia (Wilson et al., 2019), including frontotemporal dementia, dementia with Lewy bodies, and Creutzfeldt-Jakob disease (Kim et al., 2012). It is perhaps the universality of the phenomenon to various dementing disorders that makes FDG-PET a more accurate predictor of MCI-to-dementia conversion than are CSF measurements of Aβ and tau (Caminiti et al., 2018). In fact, the longitudinal decline in CMR_{glc} is associated with concurrent cognitive decline so intimately that it exceeds psychological examinationss in statistical power for monitoring longitudinal change (Landau et al., 2011). CMR_{glc} decline has been characterized as an effect of synaptic pathology, but it seems just as likely that restricted glucose delivery would be the cause of diminished mental performance, as is clearly demonstrated during acute hypoglycemic bouts (Strachan et al., 2001) and in higher performing MCI subjects (Ossenkoppele et al., 2014). Some reports indicate that CMR_{glc} is elevated before its decline in certain regions (Benzinger et al., 2013), but it is speculated that this reflects compensatory activity that is responsible for the higher cognitive performance in MCI versus AD (Ashraf et al., 2015; Ossenkoppele et al., 2014). This is not exclusive of the possibility that this elevated neurophysiological activity is, in fact, driving subsequent Aβ deposition (Cohen et al., 2009). Mice of the BRI-Aβ42 line used here have been reported to be free of cognitive impairment (Kim et al., 2013). Compared with the present study, the mice used in that report were considerably older (15 months); even the WT performed quite poorly, producing a swim-path percentage in the target quadrant scarcely better than chance (28.30 ± 2.0). It might also be noted that the mice in that study were on a mixed strain background (C57BL/6 × C3H) which may have introduced variability.

Diminished CMR_{glc} (Baker et al., 2011; Hwang et al., 2017; Roberts et al., 2014) and cognitive impairment (Biessels and Despa, 2018) are also seen in T2D. It is notable that neuron loss has not been documented in T2D. While the two conditions share some attributes, the evidence linking AD to T2D is weak. The Rush longitudinal cohort study of aging found that neither HbA1c nor diabetes was correlated with plaque, tau, or infarct pathology (Pruzin et al., 2017); cognitive and synaptic deficits in a model of T2D are independent of tau (Trujillo-Estrada et al., 2019). T2D confers no elevation in the accumulation of Aβ or neurofibrillary pathology (Beeri et al., 2005; Heitner and Dickson, 1997; Peila et al., 2002; Roberts et al., 2014). A wealth of data indicates that the greater risk for dementia among individuals with T2D can be explained adequately by the incidence of vascular dementia (above). Likewise, AD may not make a significant impact on propensity

for developing diabetes. Our study finds no convincing perturbation of fundamental endocrinology or peripheral glucose physiology in response to Aβ accumulation. This is consistent with the fact that the age-related accumulation of senile plaques in the hypothalamus does not correlate with an AD diagnosis (van de Nes et al., 1998; van de Nes et al., 2006).

Together, our findings indicate that trafficking of GLUT1 to the plasma membrane in parenchymal cells of the brain may be responsible for depressed CMR_{glc} in AD. We did not detect significant differences in steady-state levels of the total glucose transporter proteins in either $Aβ_{42}$-tg mice or human AD. Diminished overall levels of glucose transporters have been reported in other mouse models (Liu et al., 2017; Merlini et al., 2011); some evidence indicates this may represent merely a reduction in cerebrovascular mass (Ahn et al., 2018; KuznetsovaSchliebs, 2013). Increased expression of GLUT1 and −3 has also been noted in an AD model (Chua et al., 2012), potentially as a compensatory reaction to glucose starvation. Winkler et al. (2015) reported that global haploinsufficiency of GLUT1 resulted in age-related degenerative changes in the BBB, reductions in cerebral blood flow and CMR_{glc}, neurodegeneration, and memory deficits. The alterations in BBB were also noted after conditional haploinsufficiency was restricted to the vascular epithelium.

In the human brain, regional differences are more readily appreciated and may be discrepant with regard to the effects on glucose transporters by a disease process manifest in a regionally progressive pattern. Kalaria and Harik (1989) first reported that AD was accompanied by lower levels of cytochalasin B-binding sites, interpreted to be hexose transporters, in the microvessels of hippocampus; Horwood and Davies (1994) used immunohistochemistry to confirm that this likely reflected an impact on GLUT1. Vannucci et al. (1997) reported that the 45-kDa form of GLUT1 was specifically lower in AD, albeit this was limited to the caudate. Both the 45-kDa and the 55-kDa forms of the protein were found to be depleted in unspecified regions of the AD cerebral cortex by Simpson et al. (1994). Liu et al. (2008) found lower levels of both GLUT1 and GLUT3 in AD frontal cortex. We chose to analyze frontal lobe as well, hoping to avoid a high degree of late-stage neuronal loss that would be significant in the hippocampus and the temporal lobe in general. Similar to our findings in relatively young mice, human prefrontal cortex showed a reduction in plasma membrane distribution without a change in total GLUT1 levels. It is tempting to speculate that this may be an early event, occurring before the loss of overall transporter levels during the course of AD pathogenesis in a given brain region.

We also noted a reduction in total levels of GLUT2 in $Aβ_{42}$-tg mice. It is difficult to interpret this finding because there is no clear consensus on the role of GLUT2 in the brain, where it seems localized primarily to astrocytes. The K_M of GLUT2 for glucose is 15–20 mM, compared with 1–5 mM for GLUT1. Zetterling et al. (2011) reported that the concentration of glucose in human brain interstitial fluid is 0.1–5.5 mM and 1.7 ± 0.9 mM in frontal lobe. Consistent with its low affinity, GLUT2 is important for export of glucose produced by gluconeogenesis and glycogenolysis in hepatocytes. As astrocytes also store glycogen, GLUT2 could play a similar role in these cells. The fact that plasma membrane levels of GLUT2 were below the limit of detection further obscures interpretation of this transporter’s role. GLUT2 may be present only at discrete points on the astrocyte membrane,

perhaps releasing glucose from astrocytes at synapses. If this is the case, reductions in its overall levels in $A\beta_{42}$-tg brains may reflect a generalized failure in the ability of astrocytes to serve as a glucose conduit between capillaries and neurons.

Discerning the true impact of AD pathogenesis on glucose transporters may depend on a mechanistic understanding of the molecular and biochemical chain of events. Our experiments with primary cultures of astrocytes indicate that the deficit in GLUT1 localization may be a direct result of Aβ. However, proinflammatory cytokines replicated the effect of Aβ on cultured astrocytes, so it is possible that Aβ exerts an indirect effect mediated by microglial activation. Although steps were taken to diminish microglia in our primary astrocyte cultures, a few remain. Decreases in FDG-PET signal have been interpreted as a correlate of inflammatory gliosis (Schroeter et al., 2009). Intracellular trafficking of GLUT1 is not understood as well as it is for GLUT4. In many cell types, GLUT1 appears to transit through the secretory pathway in a constitutive and unregulated manner. However, there is a clear difference in the structural composition of GLUT1 in parenchymal cells, a size difference we exploited to detect differences in parenchymal transporter against the backdrop of prominent endothelial expression. It is plausible that this difference provides a mechanistic distinction in GLUT1 trafficking. It is also intriguing to speculate about the relationships between trafficking in the secretory pathway, ER stress, and metabolic syndrome, along with disturbances in autophagy. Trafficking of GLUT1 to the plasma membrane can be influenced by mammalian target of rapamycin (mTOR) (Makinoshima et al., 2015; Olsen et al., 2014), which is a major node for regulation of autophagy. *APOE* ε4, the most significant genetic factor for sporadic AD, has been demonstrated to inhibit autophagy in astrocytes (Simonovitch et al., 2016). Building on this phenomenon, we recently demonstrated a mechanistic explanation by which the gene's protein product (ApoE4) binds autophagy-gene promoters at their "CLEAR" enhancer sequences, thus competitively inhibiting the key autophagic transcription factor transcription factor EB (Parcon et al., 2018). If the resultant tendency toward protein aggregation and other forms of proteinopathy interferes with the secretory pathway, this may contribute to disturbances in localization of GLUT1 in astrocytes. A correlation between compromised CMR_{glc} and generalized astrocytic pathology has been documented in AD (Carter et al., 2019), and there is an increasing appreciation for glial contributions to such imaging modalities (Zimmer et al., 2017).

In conclusion, we found that the perturbation of glucose tolerance in $A\beta_{42}$-tg mice occurred in a manner that was independent of peripheral metabolic syndrome, hepatic glucose production, and insulin delivery or responses. This suggested an aberration in an insulin-independent tissue, such as the brain. Indeed, these mice showed a reduction in CMR_{glc} similar to human patients with AD. We further demonstrated inadequate trafficking of GLUT1 to the plasma membrane of parenchymal brain cells, likely astrocytes. Together, these data suggest that the anomalous glucose intolerance in $A\beta_{42}$-tg mice—and, potentially, humans with AD—reflects cerebrocentric effects that have little to do with endocrinological or physiological output of the hypothalamus. These findings further emphasize the growing evidence for involvement of astrocyte biology in the pathogenesis of AD. It will be important to determine where these events fit in the etiological chain of events that includes neurofibrillary pathology, tissue atrophy, and functional dementia.

Supplementary Material

Refer to Web version on PubMed Central for supplementary material.

Acknowledgements

This work was supported by the National Institutes of Health [NIA P01AG012411, NCRR P20RR020146]; The Roy and Christine Sturgis Charitable and Educational Trust; and the UAMS “S.T.O.P. Alzheimer’s” Fund. We are grateful to Dr Todd Golde (University of Florida) for providing the breeding stock of BRI-Aβ42 mice. We appreciate the technical assistance Dr Saeed Aghdam, Keri Crowder, Bounleut Phanavanh, and Sue Woodward.

References

Ahn KC, Learman CR, Dunbar GL, Maiti P, Jang WC, Cha HC, Song MS, 2018 Characterization of impaired cerebrovascular structure in APP/PS1 mouse brains. Neuroscience 385, 246–254. [PubMed: 29777753]

Alexander TC, Simecka CM, Kiffer F, Groves T, Anderson J, Carr H, Wang J, Carter G, Allen AR, 2018 Changes in cognition and dendritic complexity following intrathecal methotrexate and cytarabine treatment in a juvenile murine model. Behav. Brain Res 346, 21–28. [PubMed: 29229546]

Ashraf A, Fan Z, Brooks DJ, Edison P, 2015 Cortical hypermetabolism in MCI subjects: a compensatory mechanism? Eur. J. Nucl. Med. Mol. Imaging 42, 447–458.

Ayyadevara S, Ganne A, Hendrix RD, Balasubramaniam M, Shmookler Reis RJ, Barger SW, 2019 Functional assessments through novel proteomics approaches: application to insulin/IGF signaling in neurodegenerative disease. J. Neurosci. Methods 319, 40–46. [PubMed: 30412730]

Baker LD, Cross DJ, Minoshima S, Belongia D, Watson GS, Craft S, 2011 Insulin resistance and Alzheimer-like reductions in regional cerebral glucose metabolism for cognitively normal adults with prediabetes or early type 2 diabetes. Arch. Neurol 68, 51–57. [PubMed: 20837822]

Barros LF, Porras OH, Bittner CX, 2005 Why glucose transport in the brain matters for PET. Trends Neurosci. 28, 117–119. [PubMed: 15749163]

Beeri MS, Silverman JM, Davis KL, Marin D, Grossman HZ, Schmeidler J, Purohit DP, Perl DP, Davidson M, Mohs RC, Haroutunian V, 2005 Type 2 diabetes is negatively associated with Alzheimer’s disease neuropathology. J. Gerontol. A Biol. Sci. Med. Sci 60, 471–475. [PubMed: 15933386]

Benzinger TL, Blazey T, Jack CR Jr., Koeppe RA, Su Y, Xiong C, Raichle ME, Snyder AZ, Ances BM, Bateman RJ, Cairns NJ, Fagan AM, Goate A, Marcus DS, Aisen PS, Christensen JJ, Ercole L, Hornbeck RC, Farrar AM, Aldea P, Jasielec MS, Owen CJ, Xie X, Mayeux R, Brickman A, McDade E, Klunk W, Mathis CA, Ringman J, Thompson PM, Ghetti B, Saykin AJ, Sperling RA, Johnson KA, Salloway S, Correia S, Schofield PR, Masters CL, Rowe C, Villemagne VL, Martins R, Ourselin S, Rossor MN, Fox NC, Cash DM, Weiner MW, Holtzman DM, Buckles VD, Moulder K, Morris JC, 2013 Regional variability of imaging biomarkers in autosomal dominant Alzheimer’s disease. Proc. Natl. Acad. Sci. U S A 110, E4502–E4509. [PubMed: 24194552]

Berg JM, Tymoczko JL, Stryer L, 2002 Each Organ Has a Unique Metabolic Profile Biochemistry, fifth ed. Freeman WH, New York.

Biessels GJ, Despa F, 2018 Cognitive decline and dementia in diabetes mellitus: mechanisms and clinical implications. Nat. Rev. Endocrinol 14, 591–604. [PubMed: 30022099]

Borchelt DR, Davis J, Fischer M, Lee MK, Slunt HH, Ratovitsky T, Regard J, Copeland NG, Jenkins NA, Sisodia SS, Price DL, 1996 A vector for expressing foreign genes in the brains and hearts of transgenic mice. Genet. Anal 13, 159–163. [PubMed: 9117892]

Botteri G, Salvado L, Guma A, Lee Hamilton D, Meakin PJ, Montagut G, Ashford MLJ, Ceperuelo-Mallafre V, Fernandez-Veledo S, Vendrell J, Calderon-Dominguez M, Serra D, Herrero L, Pizarro J, Barroso E, Palomer X, Vazquez-Carrera M, 2018 The BACE1 product sAPPbeta induces ER stress and inflammation and impairs insulin signaling. Metab. Clin. Exp 85, 59–75. [PubMed: 29526536]

Boyle PJ, Kempers SF, O'Connor AM, Nagy RJ, 1995 Brain glucose uptake and unawareness of hypoglycemia in patients with insulin-dependent diabetes mellitus. N. Engl. J. Med 333, 1726–1731. [PubMed: 7491135]

Bristol WR, Drill VA, 1952 Saline hydration and diuresis after adrenalectomy. Endocrinology 50, 677–683. [PubMed: 12980076]

Caminiti SP, Ballarini T, Sala A, Cerami C, Presotto L, Santangelo R, Fallanca F, Vanoli EG, Gianolli L, Iannaccone S, Magnani G, Perani D, 2018 FDG-PET and CSF biomarker accuracy in prediction of conversion to different dementias in a large multicentre MCI cohort. NeuroImage Clin. 18, 167–177. [PubMed: 29387532]

Carter SF, Chiotis K, Nordberg A, Rodriguez-Vieitez E, 2019 Longitudinal association between astrocyte function and glucose metabolism in autosomal dominant Alzheimer's disease. Eur. J. Nucl. Med. Mol. Imaging 46, 348–356.

Chua LM, Lim ML, Chong PR, Hu ZP, Cheung NS, Wong BS, 2012 Impaired neuronal insulin signaling precedes Abeta42 accumulation in female AbetaPPsw/PS1DeltaE9 mice. J. Alzheimers Dis 29, 783–791. [PubMed: 22337827]

Cohen AD, Price JC, Weissfeld LA, James J, Rosario BL, Bi W, Nebes RD, Saxton JA, Snitz BE, Aizenstein HA, Wolk DA, Dekosky ST, Mathis CA, Klunk WE, 2009 Basal cerebral metabolism may modulate the cognitive effects of Abeta in mild cognitive impairment: an example of brain reserve. J. Neurosci 29, 14770–14778. [PubMed: 19940172]

Cornford EM, Hyman S, Cornford ME, Clare-Salzler M, 1995 Down-regulation of blood-brain glucose transport in the hyperglycemic nonobese diabetic mouse. Neurochem. Res 20, 869–873. [PubMed: 7477681]

Dienel GA, 2012 Brain lactate metabolism: the discoveries and the controversies. J. Cereb. Blood Flow Metab 32, 1107–1138. [PubMed: 22186669]

Folch J, Ettcheto M, Busquets O, Sanchez-Lopez E, Castro-Torres RD, Verdaguer E, Manzine PR, Poor SR, Garcia ML, Olloquequi J, Beas-Zarate C, Auladell C, Camins A, 2018 The implication of the brain insulin receptor in late onset Alzheimer's disease dementia. Pharmaceuticals (Basel, Switzerland) 11, 11.

Friedland RP, Budinger TF, Ganz E, Yano Y, Mathis CA, Koss B, Ober BA, Huesman RH, Derenzo SE, 1983 Regional cerebral metabolic alterations in dementia of the Alzheimer type: positron emission tomography with [18F] fluorodeoxyglucose. J. Comput. Assist. Tomogr 7, 590–598. [PubMed: 6602819]

Gabel MJ, Foster NL, Heidebrink JL, Higdon R, Aizenstein HJ, Arnold SE, Barbas NR, Boeve BF, Burke JR, Clark CM, Dekosky ST, Farlow MR, Jagust WJ, Kawas CH, Koeppe RA, Leverenz JB, Lipton AM, Peskind ER, Turner RS, Womack KB, Zamrini EY, 2010 Validation of consensus panel diagnosis in dementia. Arch. Neurol 67, 1506–1512. [PubMed: 21149812]

Gjedde A, 1981 More on the meaning of "blood-brain barrier". Clin. Chem 27, 1474.

Gjedde A, Crone C, 1981 Blood-brain glucose transfer: repression in chronic hyperglycemia. Science 214, 456–457. [PubMed: 7027439]

Hassing LB, Johansson B, Nilsson SE, Berg S, Pedersen NL, Gatz M, McClearn G, 2002 Diabetes mellitus is a risk factor for vascular dementia, but not for Alzheimer's disease: a population-based study of the oldest old. Int. Psychogeriatr 14, 239–248. [PubMed: 12475085]

Heitner J, Dickson D, 1997 Diabetics do not have increased Alzheimer-type pathology compared with age-matched control subjects. A retrospective postmortem immunocytochemical and histofluorescent study. Neurology 49, 1306–1311. [PubMed: 9371913]

Herholz K, Carter SF, Jones M, 2007 Positron emission tomography imaging in dementia. Br. J. Radiol 80 (Spec No 2), S160–S167. [PubMed: 18445746]

Hoffman JM, Welsh-Bohmer KA, Hanson M, Crain B, Hulette C, Earl N, Coleman RE, 2000 FDG PET imaging in patients with pathologically verified dementia. J. Nucl. Med 41, 1920–1928. [PubMed: 11079505]

Horwood N, Davies DC, 1994 Immunolabelling of hippocampal microvessel glucose transporter protein is reduced in Alzheimer's disease. Virchows Arch. 425, 69–72. [PubMed: 7921416]

Hwang JJ, Jiang L, Hamza M, Sanchez Rangel E, Dai F, Belfort-DeAguiar R, Parikh L, Koo BB, Rothman DL, Mason G, Sherwin RS, 2017 Blunted rise in brain glucose levels during hyperglycemia in adults with obesity and T2DM. JCI Insight 2, e95913.

Jais A, Solas M, Backes H, Chaurasia B, Kleinridders A, Theurich S, Mauer J, Steculorum SM, Hampel B, Goldau J, Alber J, Forster CY, Eming SA, Schwaninger M, Ferrara N, Karsenty G, Bruning JC, 2016 Myeloid-cell-derived VEGF maintains brain glucose uptake and limits cognitive impairment in obesity. Cell 165, 882–895. [PubMed: 27133169]

Janson J, Laedtke T, Parisi JE, O'Brien P, Petersen RC, Butler PC, 2004 Increased risk of type 2 diabetes in Alzheimer disease. Diabetes 53, 474–481. [PubMed: 14747300]

Jeon BT, Jeong EA, Shin HJ, Lee Y, Lee DH, Kim HJ, Kang SS, Cho GJ, Choi WS, Roh GS, 2012 Resveratrol attenuates obesity-associated peripheral and central inflammation and improves memory deficit in mice fed a high-fat diet. Diabetes 61, 1444–1454. [PubMed: 22362175]

Kalaria RN, Harik SI, 1989 Reduced glucose transporter at the blood-brain barrier and in cerebral cortex in Alzheimer disease. J. Neurochem 53, 1083–1088. [PubMed: 2769254]

Kasper JM, Milton AJ, Smith AE, Laezza F, Taglialatela G, Hommel JD, Abate N, 2018 Cognitive deficits associated with a high-fat diet and insulin resistance are potentiated by overexpression of ecto-nucleotide pyrophosphatase phosphodiesterase-1. Int. J. Dev. Neurosci 64, 48–53. [PubMed: 28373023]

Kim EJ, Cho SS, Jeong BH, Kim YS, Seo SW, Na DL, Geschwind MD, Jeong Y, 2012 Glucose metabolism in sporadic Creutzfeldt-Jakob disease: a statistical parametric mapping analysis of (18) F-FDG PET. Eur. J. Neurol 19, 488–493. [PubMed: 22050286]

Kim J, Chakrabarty P, Hanna A, March A, Dickson DW, Borchelt DR, Golde T, Janus C, 2013 Normal cognition in transgenic BRI2-Abeta mice. Mol. Neurodegener 8, 15. [PubMed: 23663320]

Kulas JA, Franklin W, Smith NA, Manocha GD, Puig KL, Nagamoto-Combs K, Hendrix RD, Taglialatela G, Barger SW, Combs CK, 2019 Ablation of amyloid precursor protein increases insulin Degrading enzyme levels and activity in brain and peripheral tissues. Am. J. Physiol. Endocrinol. Metab 316, E106–E120. [PubMed: 30422705]

Kuznetsova E, Schliebs R, 2013 beta-Amyloid, cholinergic transmission, and cerebrovascular system - a developmental study in a mouse model of Alzheimer's disease. Curr. Pharm. Des 19, 6749–6765. [PubMed: 23530514]

Laforce R Jr., Tosun D, Ghosh P, Lehmann M, Madison CM, Weiner MW, Miller BL, Jagust WJ, Rabinovici GD, 2014 Parallel ICA of FDG-PET and PiBPET in three conditions with underlying Alzheimer's pathology. NeuroImage Clin. 4, 508–516. [PubMed: 24818077]

Landau SM, Harvey D, Madison CM, Koeppe RA, Reiman EM, Foster NL, Weiner MW, Jagust WJ, 2011 Associations between cognitive, functional, and FDG-PET measures of decline in AD and MCI. Neurobiol. Aging 32, 1207–1218. [PubMed: 19660834]

Lee YJ, Kim JE, Hwang IS, Kwak MH, Lee JH, Jung YJ, An BS, Kwon HS, Kim BC, Kim SJ, Kim JM, Hwang DY, 2013 Alzheimer's phenotypes induced by overexpression of human presenilin 2 mutant proteins stimulate significant changes in key factors of glucose metabolism. Mol. Med. Rep 7, 1571–1578. [PubMed: 23546527]

Leuzy A, Rodriguez-Vieitez E, Saint-Aubert L, Chiotis K, Almkvist O, Savitcheva I, Jonasson M, Lubberink M, Wall A, Antoni G, Nordberg A, 2018 Longitudinal uncoupling of cerebral perfusion, glucose metabolism, and tau deposition in Alzheimer's disease. Alzheimer's & dementia. J. Alzheimers Assoc 14, 652–663.

Levites Y, Smithson LA, Price RW, Dakin RS, Yuan B, Sierks MR, Kim J, McGowan E, Reed DK, Rosenberry TL, Das P, Golde TE, 2006 Insights into the mechanisms of action of anti-Abeta antibodies in Alzheimer's disease mouse models. FASEB J. 20, 2576–2578. [PubMed: 17068112]

Li B, Matter EK, Hoppert HT, Grayson BE, Seeley RJ, Sandoval DA, 2014 Identification of optimal reference genes for RT-qPCR in the rat hypothalamus and intestine for the study of obesity. Int. J. Obes 38, 192–197.

Liu W, Zhuo P, Li L, Jin H, Lin B, Zhang Y, Liang S, Wu J, Huang J, Wang Z, Lin R, Chen L, Tao J, 2017 Activation of brain glucose metabolism ameliorating cognitive impairment in APP/PS1 transgenic mice by electroacupuncture. Free Radic. Biol. Med 112, 174–190. [PubMed: 28756309]

Liu Y, Liu F, Iqbal K, Grundke-Iqbal I, Gong CX, 2008 Decreased glucose transporters correlate to abnormal hyperphosphorylation of tau in Alzheimer disease. FEBS Lett. 582, 359–364. [PubMed: 18174027]

Lu J, Wu DM, Zheng YL, Hu B, Cheng W, Zhang ZF, Shan Q, 2011 Ursolic acid improves high fat diet-induced cognitive impairments by blocking endoplasmic reticulum stress and IkappaB kinase beta/nuclear factor-kappaB-mediated inflammatory pathways in mice. Brain Behav. Immun 25, 1658–1667. [PubMed: 21708244]

Lutz AJ, Pardridge WM, 1993 Insulin therapy normalizes GLUT1 glucose transporter mRNA but not immunoreactive transporter protein in streptozocin-diabetic rats. Metab. Clin. Exp 42, 939–944. [PubMed: 8345816]

Lyra E Silva NM, Goncalves RA, Boehnke SE, Forny-Germano L, Munoz DP, De Felice FG, 2019 Understanding the link between insulin resistance and Alzheimer's disease: Insights from animal models. Exp. Neurol 316, 1–11. [PubMed: 30930096]

Makinoshima H, Takita M, Saruwatari K, Umemura S, Obata Y, Ishii G, Matsumoto S, Sugiyama E, Ochiai A, Abe R, Goto K, Esumi H, Tsuchihara K, 2015 Signaling through the phosphatidylinositol 3-kinase (PI3K)/mammalian target of rapamycin (mTOR) axis is responsible for aerobic glycolysis mediated by glucose transporter in Epidermal growth factor receptor (EGFR)-mutated lung adenocarcinoma. J. Biol. Chem 290, 17495–17504. [PubMed: 26023239]

Matioli M, Suemoto CK, Rodriguez RD, Farias DS, da Silva MM, Leite REP, Ferretti-Rebustini REL, Pasqualucci CA, Jacob WF, Grinberg LT, Nitrini R, 2017 Association between diabetes and causes of dementia: evidence from a clinicopathological study. Dement Neuropsychol. 11, 406–412. [PubMed: 29354221]

McCall AL, Millington WR, Wurtman RJ, 1982 Metabolic fuel and amino acid transport into the brain in experimental diabetes mellitus. Proc. Natl. Acad. Sci. U S A 79, 5406–5410. [PubMed: 6752947]

McDonald JM, Cairns NJ, Taylor-Reinwald L, Holtzman D, Walsh DM, 2012 The levels of water-soluble and triton-soluble Abeta are increased in Alzheimer's disease brain. Brain Res. 1450, 138–147. [PubMed: 22440675]

McGowan E, Pickford F, Kim J, Onstead L, Eriksen J, Yu C, Skipper L, Murphy MP, Beard J, Das P, Jansen K, DeLucia M, Lin WL, Dolios G, Wang R, Eckman CB, Dickson DW, Hutton M, Hardy J, Golde T, 2005 Abeta42 is essential for parenchymal and vascular amyloid deposition in mice. Neuron 47, 191–199. [PubMed: 16039562]

McMullan SM, Phanavanh B, Li GG, Barger SW, 2012 Metabotropic glutamate receptors inhibit microglial glutamate release. ASN Neuro. 4, e00094. [PubMed: 22770428]

Merlini M, Meyer EP, Ulmann-Schuler A, Nitsch RM, 2011 Vascular beta-amyloid and early astrocyte alterations impair cerebrovascular function and cerebral metabolism in transgenic arcAbeta mice. Acta Neuropathol. 122, 293–311. [PubMed: 21688176]

Mi Y, Qi G, Fan R, Qiao Q, Sun Y, Gao Y, Liu X, 2017 EGCG ameliorates high-fat- and high-fructose-induced cognitive defects by regulating the IRS/AKT and ERK/CREB/BDNF signaling pathways in the CNS. FASEB J. 31, 4998–5011. [PubMed: 28739640]

Montine TJ, Phelps CH, Beach TG, Bigio EH, Cairns NJ, Dickson DW, Duyckaerts C, Frosch MP, Masliah E, Mirra SS, Nelson PT, Schneider JA, Thal DR, Trojanowski JQ, Vinters HV, Hyman BT, 2012 National Institute on Aging-Alzheimer's Association guidelines for the neuropathologic assessment of Alzheimer's disease: a practical approach. Acta Neuropathol. 123, 1–11. [PubMed: 22101365]

Mooradian AD, Morin AM, 1991 Brain uptake of glucose in diabetes mellitus: the role of glucose transporters. Am. J. Med. Sci 301, 173–177. [PubMed: 2000888]

Mortel KF, Wood S, Pavol MA, Meyer JS, Rexer JL, 1993 Analysis of familial and individual risk factors among patients with ischemic vascular dementia and Alzheimer's disease. Angiology 44, 599–605. [PubMed: 8342875]

Needham BE, Wlodek ME, Ciccotosto GD, Fam BC, Masters CL, Proietto J, Andrikopoulos S, Cappai R, 2008 Identification of the Alzheimer's disease amyloid precursor protein (APP) and its homologue APLP2 as essential modulators of glucose and insulin homeostasis and growth. J. Pathol 215, 155–163. [PubMed: 18393365]

Ohara T, Doi Y, Ninomiya T, Hirakawa Y, Hata J, Iwaki T, Kanba S, Kiyohara Y, 2011 Glucose tolerance status and risk of dementia in the community: the Hisayama study. Neurology 77, 1126–1134. [PubMed: 21931106]

Olsen JM, Sato M, Dallner OS, Sandstrom AL, Pisani DF, Chambard JC, Amri EZ, Hutchinson DS, Bengtsson T, 2014 Glucose uptake in brown fat cells is dependent on mTOR complex 2-promoted GLUT1 translocation. J. Cell Biol 207, 365–374. [PubMed: 25385184]

Ossenkoppele R, Madison C, Oh H, Wirth M, van Berckel BN, Jagust WJ, 2014 Is verbal episodic memory in elderly with amyloid deposits preserved through altered neuronal function? Cereb. Cortex 24, 2210–2218. [PubMed: 23537530]

Ouanes S, Popp J, 2019 High cortisol and the risk of dementia and Alzheimer's disease: a review of the literature. Front Aging Neurosci. 11, 43. [PubMed: 30881301]

Pack AI, Galante RJ, Maislin G, Cater J, Metaxas D, Lu S, Zhang L, Von Smith R, Kay T, Lian J, Svenson K, Peters LL, 2007 Novel method for high-throughput phenotyping of sleep in mice. Physiol. Genomics 28, 232–238. [PubMed: 16985007]

Parcon PA, Balasubramaniam M, Ayyadevara S, Jones RA, Liu L, Shmookler Reis RJ, Barger SW, Mrak RE, Griffin WST, 2018 Apolipoprotein E4 inhibits autophagy gene products through direct, specific binding to CLEAR motifs. Alzheimers Dement. 14, 230–242. [PubMed: 28945989]

Pardridge WM, Triguero D, Farrell CR, 1990 Downregulation of blood-brain barrier glucose transporter in experimental diabetes. Diabetes 39, 1040–1044. [PubMed: 2384187]

Peila R, Rodriguez BL, Launer LJ, 2002 Type 2 diabetes, APOE gene, and the risk for dementia and related pathologies: the Honolulu-Asia Aging Study. Diabetes 51, 1256–1262. [PubMed: 11916953]

Pruzin JJ, Nelson PT, Abner EL, Arvanitakis Z, 2018 Review: Relationship of type 2 diabetes to human brain pathology. Neuropathol. Appl. Neurobiol 44, 347–362. [PubMed: 29424027]

Pruzin JJ, Schneider JA, Capuano AW, Leurgans SE, Barnes LL, Ahima RS, Arnold SE, Bennett DA, Arvanitakis Z, 2017 Diabetes, hemoglobin A1C, and regional Alzheimer disease and infarct pathology. Alzheimer Dis. 31, 41–47.

Raffaitin C, Gin H, Empana JP, Helmer C, Berr C, Tzourio C, Portet F, Dartigues JF, Alperovitch A, Barberger-Gateau P, 2009 Metabolic syndrome and risk for incident Alzheimer's disease or vascular dementia: the Three-City Study. Diabetes Care 32, 169–174. [PubMed: 18945929]

Reno CM, Puente EC, Sheng Z, Daphna-Iken D, Bree AJ, Routh VH, Kahn BB, Fisher SJ, 2017 Brain GLUT4 Knockout mice have impaired glucose tolerance, decreased insulin sensitivity, and impaired hypoglycemic counterregulation. Diabetes 66, 587–597. [PubMed: 27797912]

Roberts RO, Knopman DS, Cha RH, Mielke MM, Pankratz VS, Boeve BF, Kantarci K, Geda YE, Jack CR Jr., Petersen RC, Lowe VJ, 2014 Diabetes and elevated hemoglobin A1c levels are associated with brain hypometabolism but not amyloid accumulation. J. Nucl. Med 55, 759–764. [PubMed: 24652830]

Schroeter M, Dennin MA, Walberer M, Backes H, Neumaier B, Fink GR, Graf R, 2009 Neuroinflammation extends brain tissue at risk to vital peri-infarct tissue: a double tracer [11C]PK11195- and [18F]FDG-PET study. J. Cereb. Blood Flow Metab 29, 1216–1225. [PubMed: 19352400]

Simonovitch S, Schmukler E, Bespalko A, Iram T, Frenkel D, Holtzman DM, Masliah E, Michaelson DM, Pinkas-Kramarski R, 2016 Impaired autophagy in APOE4 astrocytes. J. Alzheimers Dis 51, 915–927. [PubMed: 26923027]

Simpson IA, Chundu KR, Davies-Hill T, Honer WG, Davies P, 1994 Decreased concentrations of GLUT1 and GLUT3 glucose transporters in the brains of patients with Alzheimer's disease. Ann. Neurol 35, 546–551. [PubMed: 8179300]

Sokoloff L, 1977 Relation between physiological function and energy metabolism in the central nervous system. J. Neurochem 29, 13–26. [PubMed: 407330]

Strachan MW, Deary IJ, Ewing FM, Ferguson SS, Young MJ, Frier BM, 2001 Acute hypoglycemia impairs the functioning of the central but not peripheral nervous system. Physiol. Behav 72, 83–92. [PubMed: 11239984]

Thambisetty M, Jeffrey Metter E, Yang A, Dolan H, Marano C, Zonderman AB, Troncoso JC, Zhou Y, Wong DF, Ferrucci L, Egan J, Resnick SM, O'Brien RJ, 2013 Glucose intolerance, insulin

resistance, and pathological features of Alzheimer disease in the Baltimore Longitudinal Study of Aging. JAMA Neurol. 70, 1167–1172. [PubMed: 23897112]

Trujillo-Estrada L, Nguyen C, da Cunha C, Cai L, Forner S, Martini AC, Ager RR, Prieto GA, Cotman CW, Baglietto-Vargas D, LaFerla FM, 2019 Tau underlies synaptic and cognitive deficits for type 1, but not type 2 diabetes mouse models. Aging Cell 18, e12919. [PubMed: 30809950]

Tu Z, Keller MP, Zhang C, Rabaglia ME, Greenawalt DM, Yang X, Wang IM, Dai H, Bruss MD, Lum PY, Zhou YP, Kemp DM, Kendziorski C, Yandell BS, Attie AD, Schadt EE, Zhu J, 2012 Integrative analysis of a cross-loci regulation network identifies App as a gene regulating insulin secretion from pancreatic islets. PLoS Genet. 8, e1003107. [PubMed: 23236292]

Vallerand AL, Perusse F, Bukowiecki LJ, 1987 Cold exposure potentiates the effect of insulin on in vivo glucose uptake. Am. J. Physiol 253, E179–E186. [PubMed: 3303966]

van de Nes JA, Kamphorst W, Ravid R, Swaab DF, 1998 Comparison of beta-protein/A4 deposits and Alz-50-stained cytoskeletal changes in the hypothalamus and adjoining areas of Alzheimer's disease patients: amorphic plaques and cytoskeletal changes occur independently. Acta Neuropathol. 96, 129–138. [PubMed: 9705127]

van de Nes JA, Konermann S, Nafe R, Swaab DF, 2006 Beta-protein/A4 deposits are not associated with hyperphosphorylated tau in somatostatin neurons in the hypothalamus of Alzheimer's disease patients. Acta Neuropathol. 111, 126–138. [PubMed: 16456666]

Vannucci SJ, Maher F, Simpson IA, 1997 Glucose transporter proteins in brain: delivery of glucose to neurons and glia. Glia 21, 2–21. [PubMed: 9298843]

Wilson H, Pagano G, Politis M, 2019 Dementia spectrum disorders: lessons learnt from decades with PET research. J. Neural Transm. (Vienna) 126, 233–251. [PubMed: 30762136]

Winkler EA, Nishida Y, Sagare AP, Rege SV, Bell RD, Perlmutter D, Sengillo JD, Hillman S, Kong P, Nelson AR, Sullivan JS, Zhao Z, Meiselman HJ, Wendy RB, Soto J, Abel ED, Makshanoff J, Zuniga E, De Vivo DC, Zlokovic BV, 2015 GLUT1 reductions exacerbate Alzheimer's disease vasculo-neuronal dysfunction and degeneration. Nat. Neurosci 18, 521–530. [PubMed: 25730668]

Zetterling M, Hillered L, Enblad P, Karlsson T, Ronne-Engstrom E, 2011 Relation between brain interstitial and systemic glucose concentrations after subarachnoid hemorrhage. J. Neurosurg 115, 66–74. [PubMed: 21476811]

Zimmer ER, Parent MJ, Souza DG, Leuzy A, Lecrux C, Kim HI, Gauthier S, Pellerin L, Hamel E, Rosa-Neto P, 2017 [(18)F]FDG PET signal is driven by astroglial glutamate transport. Nat. Neurosci 20, 393–395. [PubMed: 28135241]

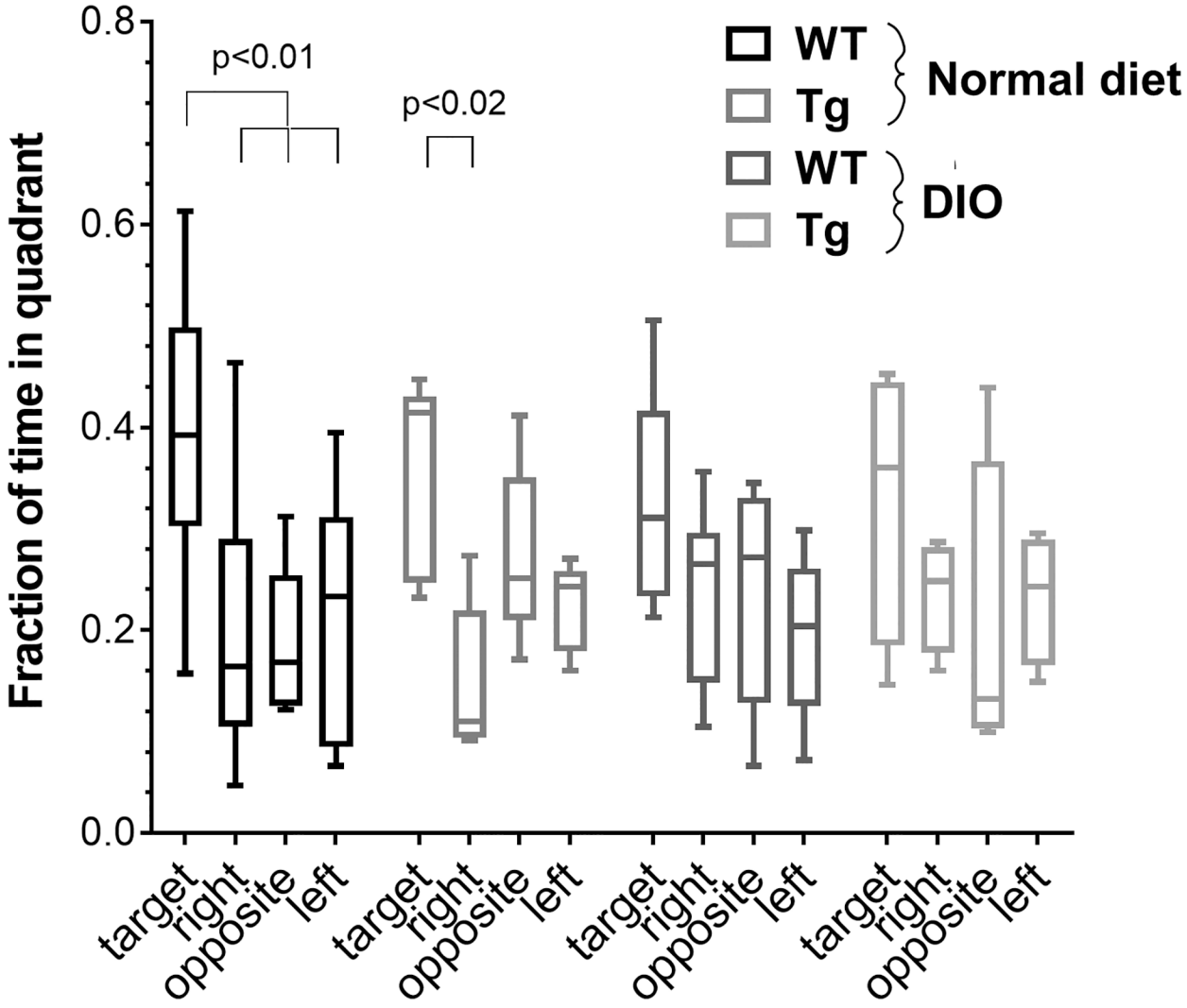

Fig. 1.

Cerebral Aβ accumulation and western diet impaired spatial memory. $A\beta_{42}$-tg mice ("Aβ-tg") and wild-type littermates ("WT") were maintained on normal diet (ND); additional mice of each genotype were also subjected to 6 weeks of DIO. The mice were trained in the MWM task and tested in a probe trial on day 6. Values represent the percentage of time spent in each quadrant of the pool during the probe trial. WT ND males spent significantly more time in the target quadrant than in any other quadrant, indicating retention of training (*$p \leq 0.05$, **$p \leq 0.01$).

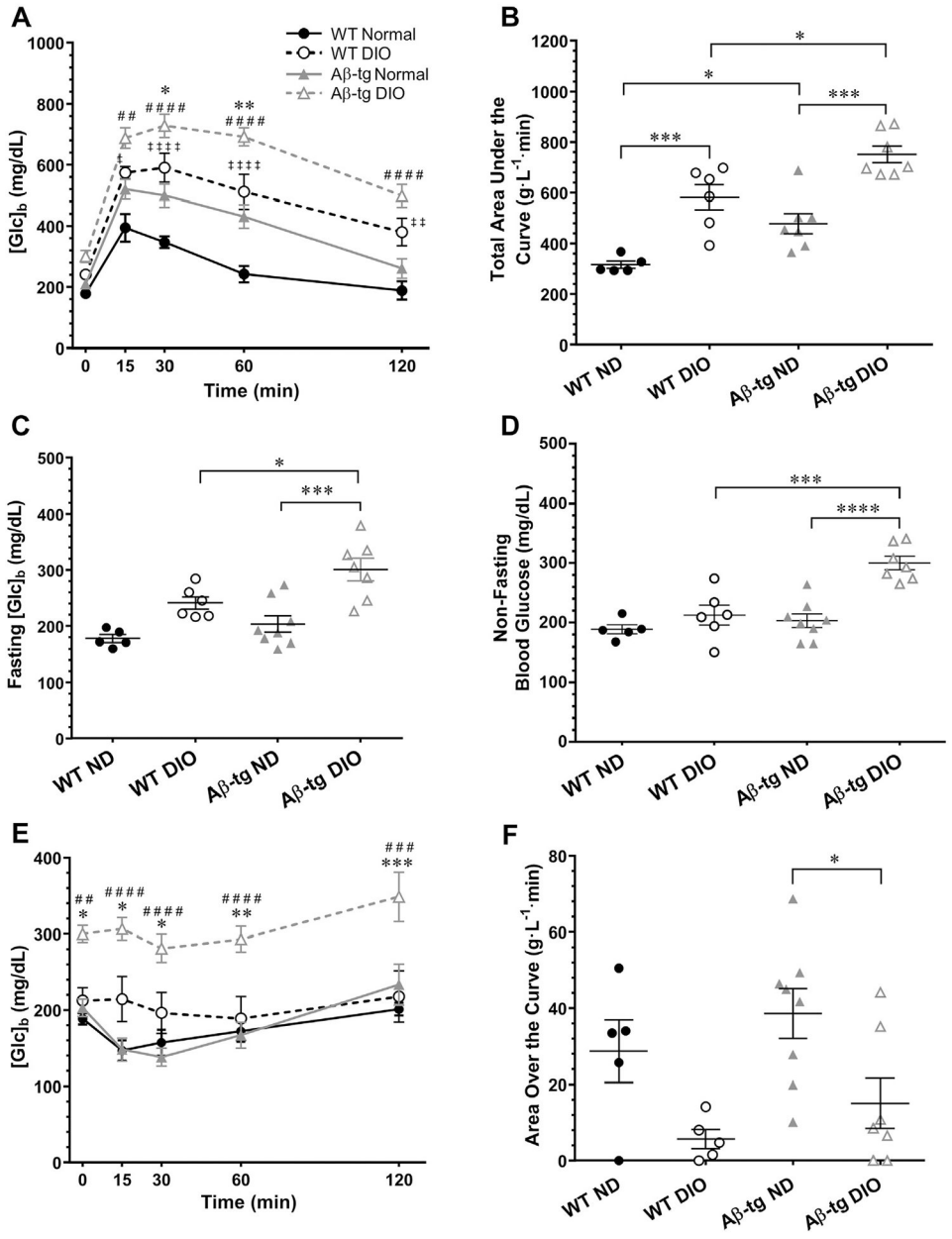

Fig. 2.

Peripheral glucose tolerance was impaired in Aβ$_{42}$-tg mice. Glucose tolerance testing (GTT) and insulin tolerance testing (ITT) were performed on Aβ$_{42}$-tg mice ("Aβ-tg") and WT littermates on a ND or western diet (DIO) for 9 weeks. A: On both diets, Aβ$_{42}$-tg mice had significantly higher $[Glc]_b$ than WT at 30 and 60 minutes (*$p < 0.05$, **$p < 0.01$). DIO elevated $[Glc]_b$ levels within both genotypes (WT Normal vs. WT DIO: $^{‡‡}P < 0.01$, $^{‡‡‡‡}P < 0.0001$; Aβ-tg Normal vs. Aβ-tg DIO: $^{\#\#}p < 0.01$, $^{\#\#\#\#}p < 0.0001$). B: DIO increased total area under the curve (tAUC) in the GTT (***$p < 0.001$). Aβ$_{42}$-tg mice had greater tAUC than WT on the same diet (*$p < 0.05$). C, D: Fasting and nonfasting basal $[Glc]_b$ were higher in Aβ-tg DIO than in either WT DIO or Aβ-tg ND (*$p < 0.05$, ***$p < 0.001$, ****$p < 0.0001$). E: ITT showed that the Aβ-tg DIO group had a significantly greater impairment

than WT DIO (*$p < 0.05$, **$p < 0.01$, ***$p < 0.001$), but Aβ-tg ND was not different from WT ND. F: AOC in the ITT indicated that the WT DIO group had impaired responses to insulin compared with WT ND, and Aβ-tg DIO also showed impairment (*$p < 0.05$). All values are mean ± SEM.

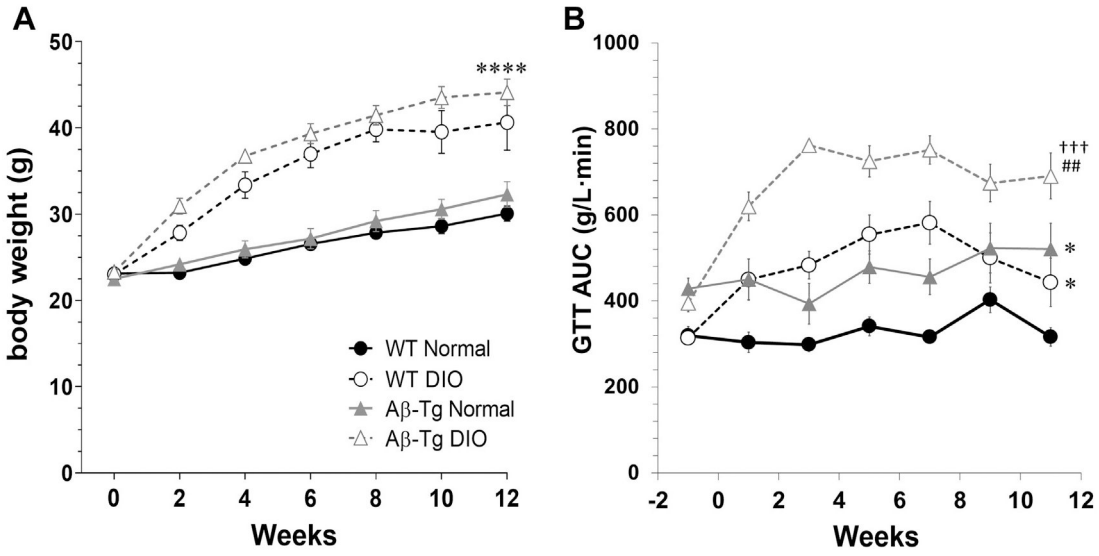

Fig. 3.

Progressive changes in DIO paradigm. $A\beta_{42}$-tg and WT littermates were fed a ND or western diet for 12 weeks (reflected in the abscissa label). A: Mice were weighed biweekly without fasting (****$p < 0.0001$ each DIO group vs. its ND counterpart). B: GTT was performed on weeks alternating with the body weight measurements. (*$p \leq 0.03$ vs. WT Normal, $^{\#\#}p < 0.002$ Aβ-tg Normal, $^{\dagger\dagger\dagger}p = 0.0005$ vs. WT DIO).

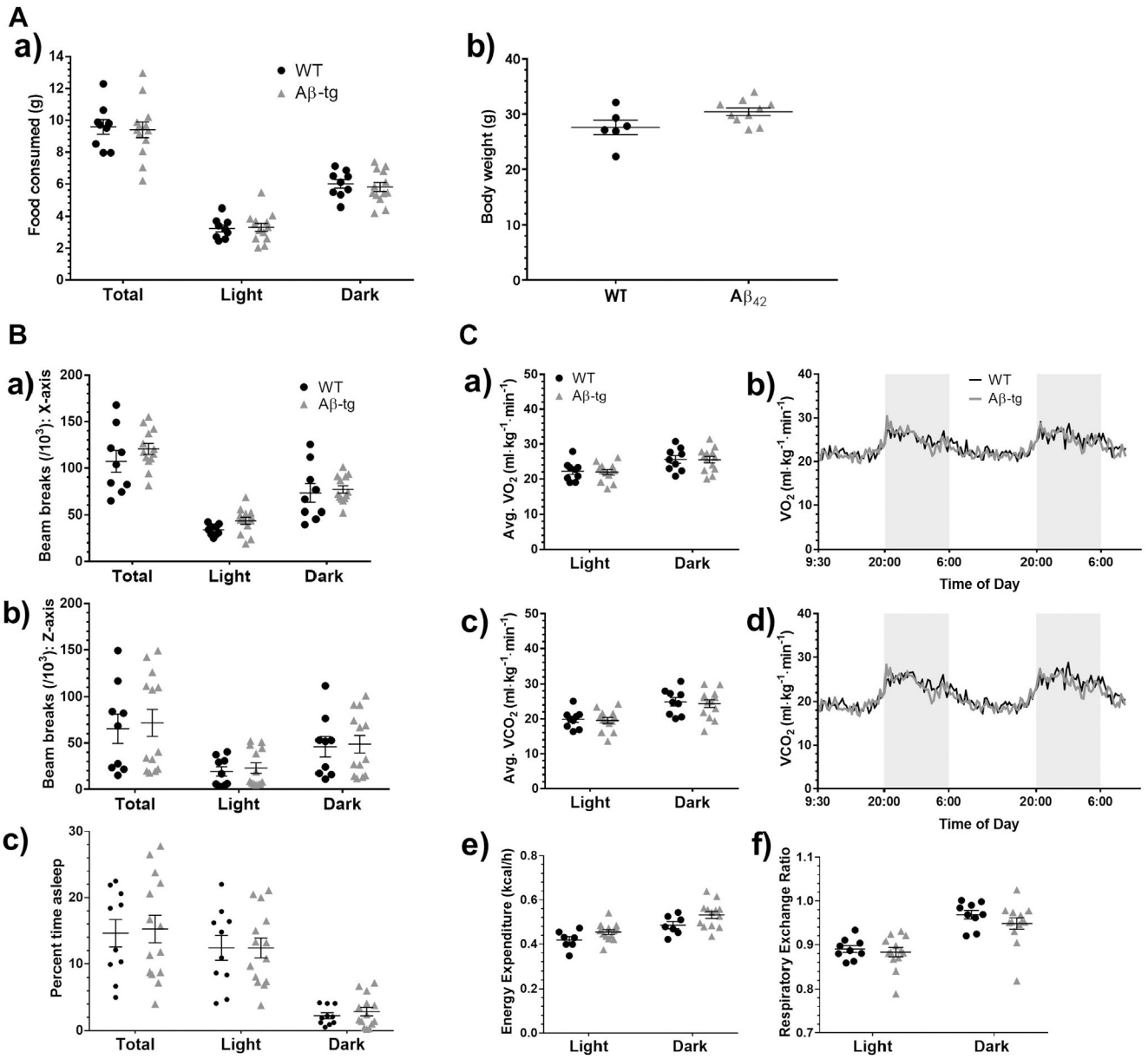

Fig. 4.

$A\beta_{42}$-tg mice show no aberrations in food consumption, body weight, physical activity, or respiration. $A\beta_{42}$-tg mice and WT littermates were acclimated to CLAMS cages and then monitored for 48 hours. A: $A\beta_{42}$-tg mice consumed an equivalent mass of food (a) during light and dark hours; they also achieved similar body weights (b). B: Monitoring of activity with infrared beams during light and dark hours indicated no difference between genotypes in ambulation, as indicated by movement in the x-axis (a), or in jumping/rearing, as indicated by movement in the z-axis (b); sleep time (c) was derived from the movement data and also showed no differences. C: Consumption of O_2 (a, b) and production of CO_2 (c, d) was monitored, indicating no genotypic differences in these primary measures or in the calculations of energy expenditure (e) or respiratory exchange ratio (f).

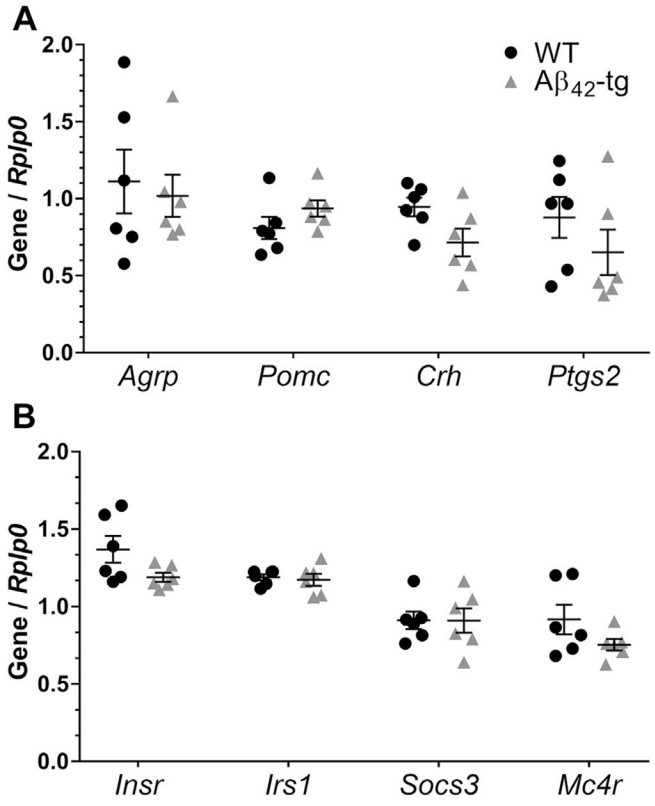

Fig. 5.

Hypothalamic gene expression in 28-week-old WT and $A\beta_{42}$-overexpressing mice. Hypothalamus tissues from fasted mice that were 28 weeks of age were homogenized, and mRNA was extracted. A: Using qRT-PCR (see "Methods"); *Agrp*, *Pomc*, *Crh*, and *Ptgs2* gene expression were normalized to the stable transcript *Rplp0*. B: *Insr*, *Irs1*, *Socs3*, and *Mc4r* expression was normalized using *Rplp0* and showed no differences. Comparisons were evaluated using Student's *t*-test with Welch's correction. All values are mean ± SEM.

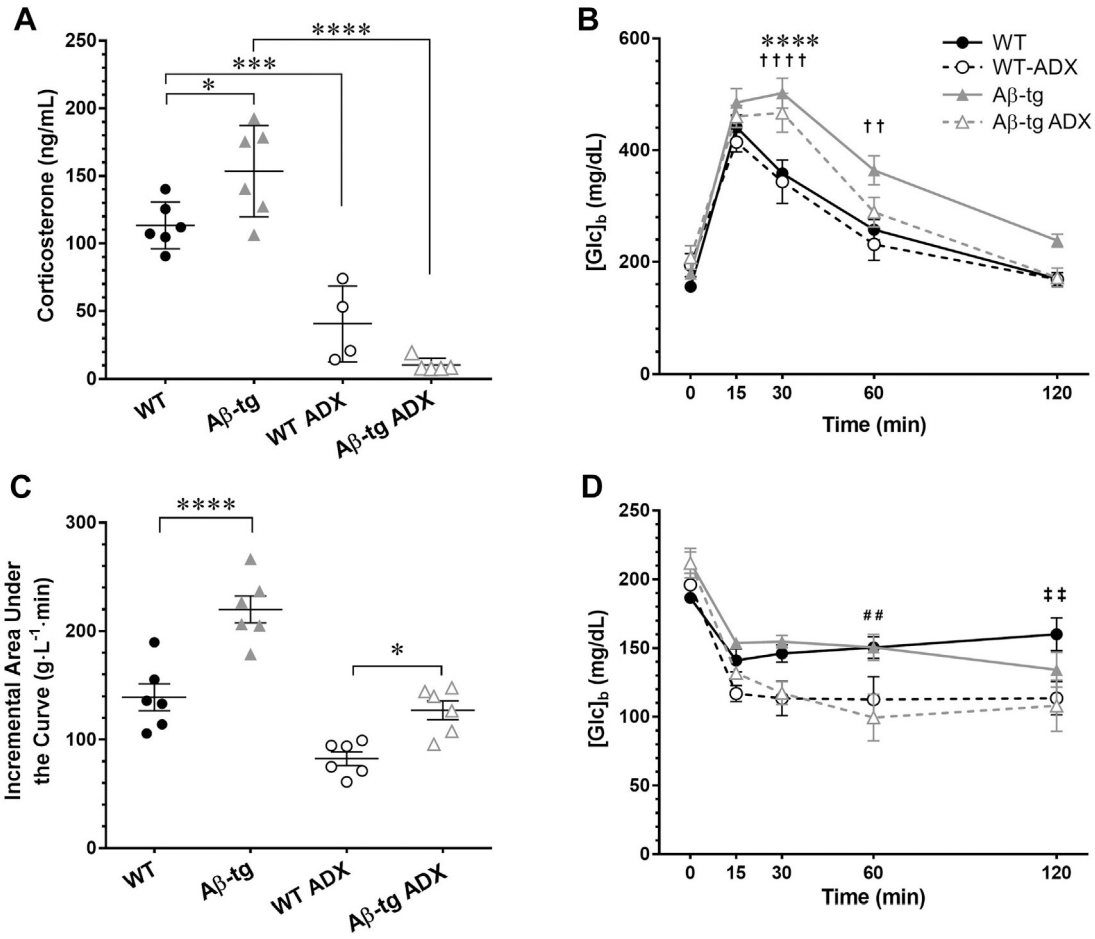

Fig. 6.

$A\beta_{42}$-tg mice retain impaired glucose tolerance after adrenalectomy. GTT was performed on mice 19 days after adrenalectomy (ADX), and insulin tolerance testing ITT was performed the following week. WT adrenalectomized (WT-ADX) and $A\beta_{42}$-tg adrenalectomized ($A\beta_{42}$-ADX) mice were compared with WT and $A\beta_{42}$-tg unoperated littermates. A: After a 5-h fast, corticosterone was measured in serum. Adrenalectomy decreased corticosterone levels in WT animals (***$p < 0.001$) and $A\beta_{42}$-tg animals (****$p < 0.0001$); unoperated $A\beta_{42}$-tg mice had increased corticosterone relative to unoperated WT (*$p < 0.05$). B: GTT indicated that $[Glc]_b$ was elevated in $A\beta_{42}$-tg more than in WT at 30 and 60 minutes ($^{††}p < 0.01$, $^{††††}p < 0.0001$). $A\beta_{42}$-ADX had significantly higher $[Glc]_b$ than WT-ADX at 30 minutes (****$p < 0.0001$). C: $A\beta_{42}$-tg had higher AUC values than WT in the unoperated group (****$p < 0.0001$) and in the ADX group (*$p < 0.05$). D: Adrenalectomized mice trended toward greater insulin sensitivity ($A\beta_{42}$ vs. $A\beta_{42}$-ADX: $^{\#\#}p < 0.01$, WT vs. WT-ADX: $^{‡‡}p < 0.01$). All values are mean ± SEM.

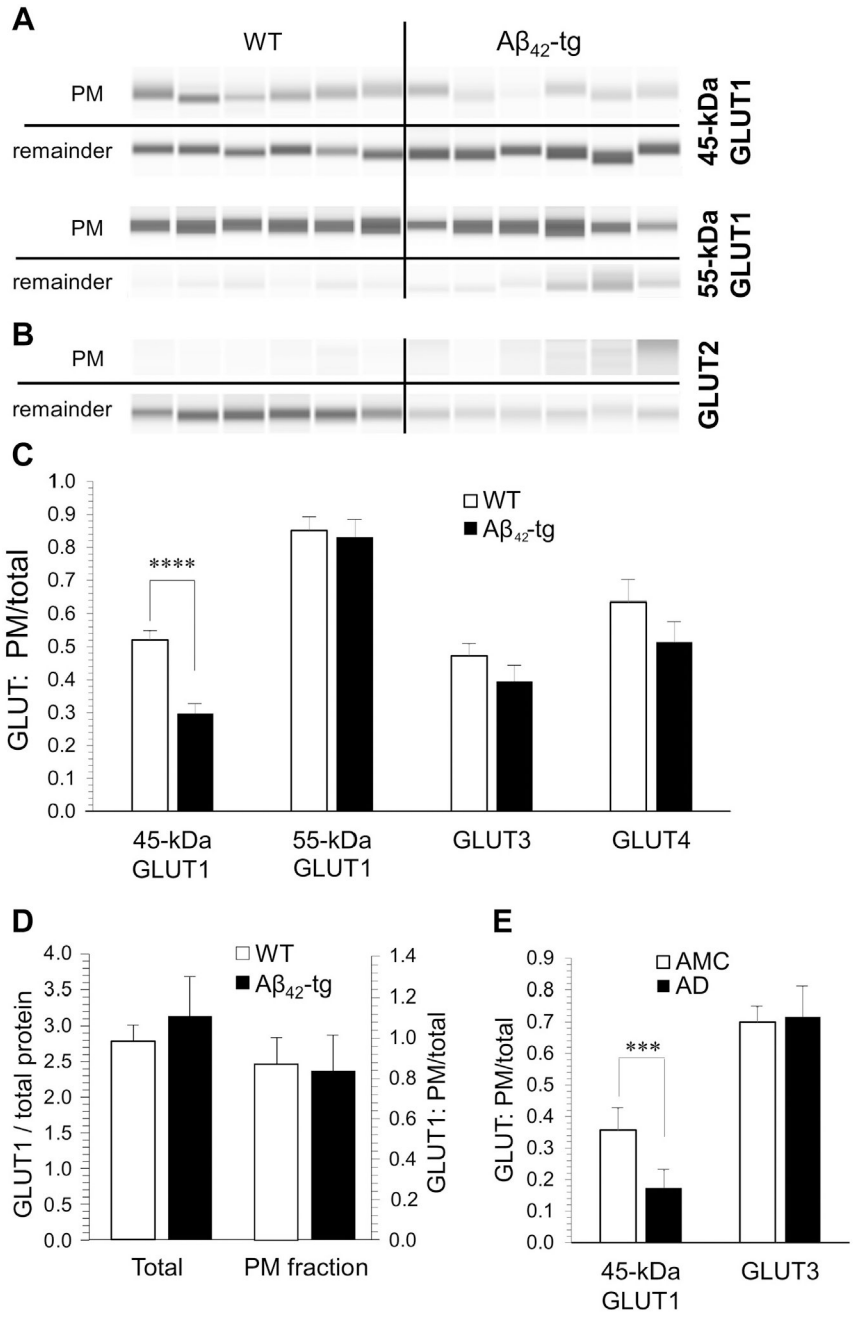

Fig. 7.

GLUT1 fractional distribution to the plasma membrane was perturbed in $A\beta_{42}$-tg mice and AD cortex. Homogenates from cerebral cortex were fractionated to separate plasma membrane (PM) from the other cellular fractions ("remainder"), then samples normalized for protein content were resolved by capillary electrophoresis, and GLUT proteins were detected by antibody-dependent chemiluminescence. A: Pseudogel depiction of the scans of 45-kDa and 55-kDa GLUT1 detection in whole cerebrum from WT and $A\beta_{42}$-tg mice. (Small discrepancies in vertical position reflect idiosyncracies among the capillaries and are common with this technology.) B: Pseudogel depiction of GLUT2 PM and remainder

fractions in whole cerebrum from WT and $A\beta_{42}$-tg mice. C: Quantification of the PM fractional value ("total" = PM + remainder) for the indicated proteins in whole cerebrum from WT and $A\beta_{42}$-tg mice. D: Quantification of total GLUT1 (left ordinate; normalized to total protein) and PM fractional value of GLUT1 (right ordinate) from cerebral microvessel isolates. D: Quantification of the PM fractional value ("total" = PM + remainder) for the indicated proteins from human subjects diagnosed with AD or no neurological disease (age-matched controls, AMC). All values are mean ± SEM.

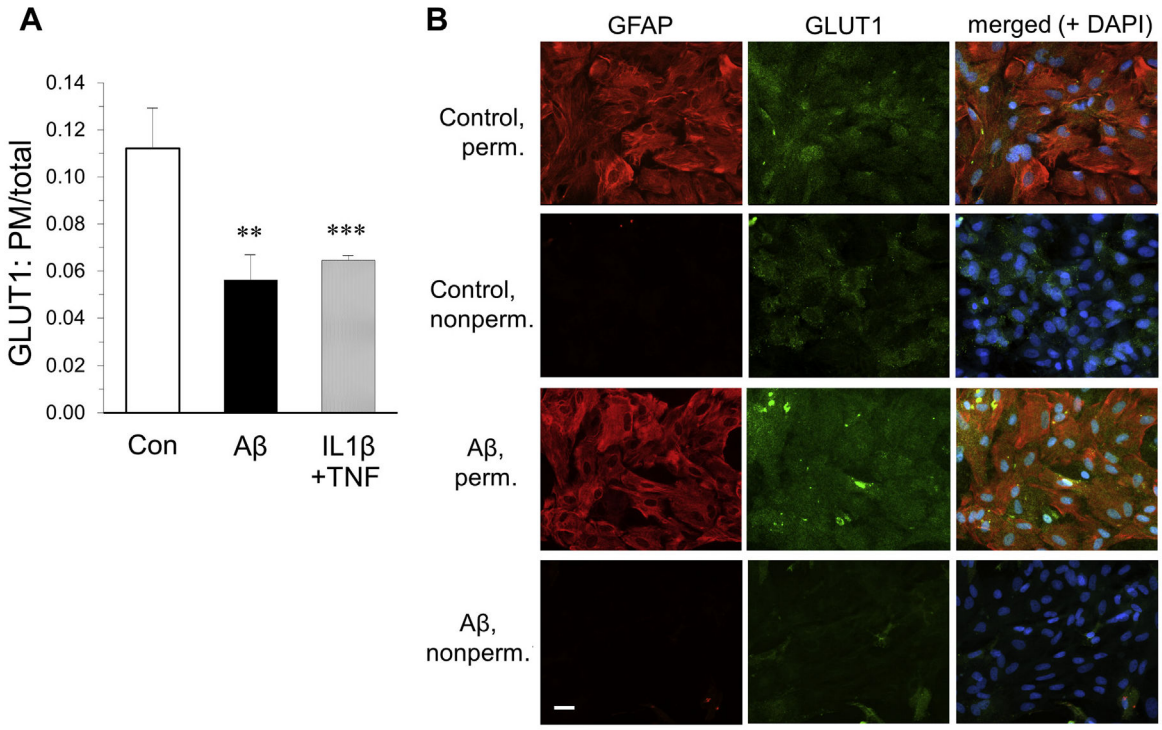

Fig. 8.

Aβ and cytokines evoke aberrant trafficking of GLUT1 in cultured astrocytes Primary cultures of astrocytes were treated 6 hours with aggregated $A\beta_{1–42}$ (2.5 μM) or 4 hours with a combination of IL1β and TNF (10 and 30 ng/mL, respectively). A: PM fractional value of 45-kDa GLUT1 detected by capillary-gel immunodetection as in Fig. 7. B: Immunofluorescence of GLUT1 and GFAP performed on cultures that had been permeabilized or not before application of primary antibodies. Absence of GFAP staining in unpermeabilized cells validates that GLUT1 staining in those cultures is likely restricted to cell-surface protein. Scale bar = 25 μm.

Table 1

Insulin levels impacted by diet but not genotype

Mouse group		**[Insulin] (ng/mL)**					
Genotype	**Diet (6 wk)**	**T_0**		**T_{30}** *a*		**%Δ**	
WT (littermates)	normal	0.474	±0.043	1.07	±0.179 *b*	125.8	±27.94
	western	2.66	±0.547	2.80	±0.789	22.26	±31.43
$A\beta_{42}$-tg	normal	0.553	±0.107	1.10	±0.173 *b*	147.4	±53.75
	western	5.78	±2.03	3.74	±1.42	−17.69	±24.21

a 30 min after challenge with glucose (2 g/kg body wt.).

b $p \leq 0.01$ versus T_0.